Statistical behavior of nucleon transfer to highly excited states in heavy-ion collisions

J. S. Karp,* S. G. Steadman, S. B. Gazes, and R. Ledoux
Laboratory for Nuclear Science and Physics Department, Massachusetts Institute of Technology, Cambridge, Massachusetts 02139

F. Videbæk
Niels Bohr Institute, Copenhagen, Denmark and Laboratory for Nuclear Science, Massachusetts Institute of Technology, Cambridge, Massachusetts 02139

(Received 25 November 1981)

The Q-value dependence of the cross section of heavy-ion transfer reactions to high-lying states is studied. The continuum energy spectra are measured for each exit channel while systematically varying the bombarding energy, scattering angle, target and projectile: $^{16}O + ^{232}Th$, $^{15}N + ^{232}Th$ and ^{181}Ta, and $^{35}Cl + ^{181}Ta$ at energies ranging up to 1.4 times the Coulomb barrier, at and about the grazing angle. The transfer reactions exhibit common properties which depend mainly on the number of transferred nucleons ΔN. The average amount of energy dissipated, which depends strongly on ΔN, is interpreted with a semiclassical model that assumes momentum matching and the presence of a velocity-dependent frictional force. Also, the branching ratios of the exit channels are observed to depend systematically on ΔN, which suggests a statistical process. The energy spectra are examined in terms of a phenomenological constrained phase-space analysis. The dominant constraint is found to be the optimal Q value. The description of data with at most two constraints implies that essentially all of the information content of the energy distribution is contained in these constraints.

[NUCLEAR REACTIONS Heavy ions, $^{232}Th(^{16}O,X)$, $X=^{9,10}Be$, $^{11-13}B$, $^{12-16}C$, $^{15-17}N$, $^{17-19}O$, $E=97,105,115,125$ MeV. ^{181}Ta, $^{232}Th(^{15}N,X)$, $X=^{9-11}Be$, $^{11-13}B$, $^{12-15}C$, $E=86,95,103$ MeV. $^{181}Ta(^{35}Cl,X)$, $X=^{30-32}Si$, $^{31-34}P$, $^{33-36}S$, $^{36,37}Cl$, $E=205$ MeV. Energy and angular distributions of the ejectiles. Statistical aspects. Surprisal analysis.]

I. INTRODUCTION

This paper examines the continuum energy spectra and other general properties of transfer reactions to the continuum in a systematic manner, since many existing measurements are rather fragmentary. Often, the features of heavy-ion reactions appear to be particular to individual reactions, whereas in fact many are general characteristics depending on the relative kinetic energy and angular momentum of the dinuclear system, which evolves in time from the regime of direct processes to that of statistical processes. This transition can be effectively studied by varying the incident parameters in modest steps and observing the changes in the final distributions, including those of energy, angle, mass, and charge.

Both direct reaction and statistical diffusion theories have been applied to understand continuum energy spectra in quasielastic and deep-inelastic collisions. Distorted-wave Born approximation (DWBA) cross sections have been calculated using energy averaged matrix elements by Udagawa *et al.*[1] for the direct reaction products of $^{14}N+^{92}Mo$ at 97 MeV. The theoretical fits account for the peak positions and widths of the energy spectra, but do not correctly describe their shape. The failure to reproduce the cross section at high excitation energies is probably due to the neglect of multistep processes. Taking advantage of the large number of degress of freedom, a statistical diffusion model has been applied by Nörenberg[2] to the continuum energy spectra of the $^{40}Ar+^{232}Th$ reaction

at 388 MeV. Here, the drift of the energy peak and diffusive broadening of the energy distributions are seen as the interaction time increases, although the observed asymmetries, especially for weakly damped or few-nucleon transfers, are unaccounted for. Volkov[3] treats deep-inelastic reactions in terms of an intermediate dinuclear system, which makes it possible to interpret some features of multinucleon transfer by a statistical approach; for example, the ground state Q-value (Q_0) systematics seen by Artukh *et al.*[4] Bondorf *et al.*[5] explain the logarithmic dependence of the cross section with Q_0 to be a consequence of partial statistical equilibrium. During the relatively fast transfer reaction, the system of colliding ions is restricted to a subset of the degrees of freedom and thus to a fraction of the total available phase space. The cross section, with respect to energy and nucleon exchange, is then proportional to the phase space, which is approximated by the nuclear level density of a Fermi gas with a reduced level density parameter a. Calculated isotope yields $d\sigma/d\Omega$ are in qualitative agreement with the observations of Ref. 4. On the other hand, Lee and Braun-Munzinger[6] explain these yields in terms of a direct reaction mechanism.

The validity of a statistical approach to the continuum energy spectra of transfer reactions is examined in this paper, though in a somewhat different context from the diffusion theories. The energy spectra have been very well described by Levine *et al.*[7] using the concepts of the maximal entropy formalism (known as surprisal analysis). The measured energy spectra of the exit channels of the $^{16}O+^{232}Th$ grazing reaction, as well as other transfer reactions,[8] are fit with this constrained phase-space approach, where the average energy is determined to be the dominant constraint of the reaction. Thus, the energy spectrum is the statistically most probable distribution, yet constrained to peak about some optimal energy. The energy loss that accompanies mass transfer is an important feature of heavy-ion transfer reactions. The rate of loss depends on the evolution of the reaction and the mechanism of nucleon exchange. Apart from being constrained by the average energy, it is surprising that the energy distribution can nevertheless be described so statistically.

It is of interest to determine whether surprisal analysis works for reactions other than $^{16}O+^{232}Th$ and, of course, how much can be learned from this approach. Part of the motivation for this work, which constitutes a Ph.D. thesis[9] of one of the authors, was to ascertain the validity of surprisal analysis as a general description of continuum energy spectra of transfer reactions.

Transfer reactions can be studied with almost any combination of projectile and target. However, this work confines itself to highly asymmetric systems with lighter projectiles on heavier targets. The most important reason for studying highly asymmetric systems is that evaporation from the projectile is minimal. The excitation energy is predominantly in the heavier nucleus which has a much higher level density, thus many more degrees of freedom. Consequently, it is unlikely for the light ejectile to evaporate a particle that would change its identity before it is detected.

The grazing reaction $^{16}O+^{232}Th$ was studied in detail because of its large mass asymmetry as well as for the following considerations. This transfer reaction is focused at the grazing angle for a narrow region of impact parameters; hence, the transfer cross section is maximal there. Only a few partial waves contribute to the transfer cross section, strongly selecting the initial condition. Yet, there is still a considerable amount of energy damping. For one- or two-nucleon transfer up to about one-half the incident kinetic energy above the Coulomb barrier is dissipated into internal energy, while for six- or seven-nucleon transfer almost all is dissipated. Nevertheless, a relatively modest amount of angular momentum is transferred, which imparts only a small rotational energy to the heavy nucleus compared to the internal excitation energy. Hence, the effects of transferred energy can be isolated from those of transferred angular momentum. Finally, for these reactions above the Coulomb barrier, the excitation energy is high enough to consider the excited nucleus to be in the continuum.

Thus, this paper investigates reactions with a variety of initial conditions by measuring the final distributions which depend on the mechanism of nucleon exchange. The general properties of the reaction and their dependence on bombarding energy, scattering angle, and entrance channel are studied. The constrained phase-space approach is shown to provide an accurate description of the continuum energy spectra with at most two contraints for this variety of bombarding conditions.

The experimental setups, including the counter telescope method and time-of-flight method, are described in Sec. II. The data and a discussion of the results follow in Sec. III. Section IV treats the application of surprisal analysis to the energy spectra. Finally, the paper is summarized with concluding remarks in Sec. V.

II. EXPERIMENTAL SETUP

A. Introduction

The data were taken at the Brookhaven National Laboratory Tandem Van de Graaff Accelerator facility operated in the three-stage configuration. Reactions with ^{16}O used E-ΔE solid state counter telescopes to determine the energy, mass, and charge of the light ejectiles for each exit channel of the transfer reaction. The $^{16}O+^{232}Th$ reaction at 105 MeV was studied most thoroughly. An elastic scattering angular distribution was measured to determine the reaction cross section, as well as the grazing partial wave and strong absorption radius. Doubly differential cross sections as a function of scattering angle and Q value were measured to extract the dependence of the energy spectra on scattering angle, as well as to obtain the angle-integrated cross sections. The dependence of the energy spectra on bombarding energy was also investigated, at and about the grazing angle. The energies ranged from the Coulomb barrier to the maximum BNL could produce, about 125 MeV for ^{16}O. Finally, the entrance channel was varied; the projectile ^{15}N was bombarded on ^{232}Th and ^{181}Ta for a variety of incident energies and scattering angles.

The counter telescope procedure works well for oxygenlike ejectiles, as long as the electronic system is carefully tuned up for optimum energy resolution, which in turn determines the mass resolution. For heavier nuclei, such as ^{35}Cl, a clear separation of the different isotopes is no longer possible. Therefore, a large-solid-angle parallel-plate gas-ionization chamber was developed for use in conjunction with the BNL time-of-flight (TOF) setup. The $^{16}O+^{232}Th$ system at 105 MeV incident energy was remeasured to compare with and supplement the counter telescope data, followed by a measurement of the $^{35}Cl+^{181}Ta$ system at the same relative velocity.

B. Counter telescope data

An example of a counter telescope E_T-ΔE density plot is shown in Fig. 1 for the reaction $^{16}O+^{232}Th$ at an incident energy of 105 MeV. The telescope, placed at $\theta_{lab}=70°$, consisted of a 30 μm ΔE totally depleted silicon surface-barrier (SSB) detector and a 60 μm E partially depleted SSB detector, both 100 mm^2 in area. The masses as well as the charges are very well separated, allowing one to identify adjacent isotopes. Here, the finite thickness ΔX of the ΔE detector determines the low energy cutoff for each ion as that energy whose range is ΔX. There happens to be a slight high energy cutoff only for the lightest beryllium ions, because the 60 μm thick E detector is not thick enough to stop these ions at the highest energies. Subsequent experiments used 30 μm ΔE detectors and 300 μm E detectors, all 50 mm^2 in area.

Typically, the solid angle subtended by the telescope was 4 msr, with an opening angle of 2° as defined by a 6 mm diameter bevelled collimator. The cross sections were normalized by a monitor detector placed at 20°. The thorium and tantalum targets, both rolled, were about 1 mg/cm^2 and 0.5 mg/cm^2, respectively. Neither the finite target thickness nor the finite solid angle of the telescope significantly affected the energy resolution, which was measured to be about 1% for the summed energy signal.

The E_T-ΔE spectra were collected in 128×256 matrices. The FWHM of a mass group is about six channels, which allows separation of the isotopes (see Fig. 1), allowing projection of each group onto the energy axis. The peak-to-valley ratio in Fig. 1 is

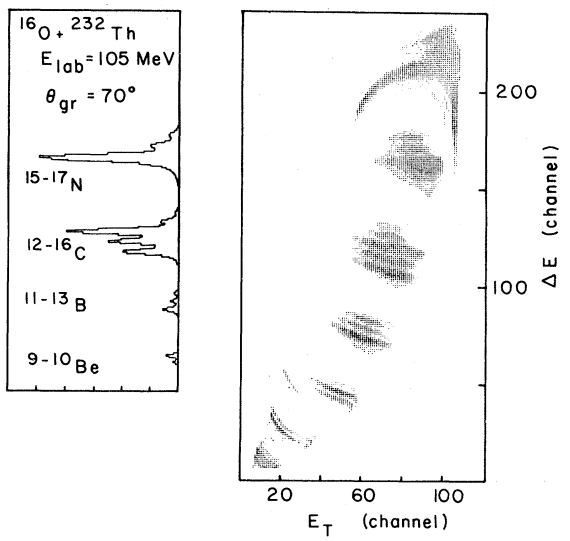

FIG. 1. Density plot of specific energy loss versus total energy for scattered projectilelike products from the $^{16}O+^{232}Th$ reaction at the grazing angle of 70° at 105 MeV incident energy. A projection of the mass and charge groups is shown to the left. These data were obtained using the counter telescope.

seen to be about 5:1 at its best. So, the projection procedure is somewhat imprecise, especially for the least dominant isotope of a given charge. However, several reactions were repeated at different times, so that independent energy calibrations and isotope separations were done. The results are consistent, with an uncertainty less than 8% in the number of counts of the energy projection for each isotope. Since the statistical uncertainty is small for a measurement with many thousands of counts, the error is primarily due to the incomplete mass separation. The centroid of the energy distribution has an uncertainty of only about $1\frac{1}{2}\%$, including the uncertainties in the energy calibrations that varied between runs. The calibrations were made from elastic scattering measurements at several bombarding energies. The excitation energy is computed from the calibrated kinetic energy, with the ground state Q value evaluated using the mass tables of Wapstra and Gove.[10]

C. Time-of-flight method

The TOF system at BNL consists of a 30 cm diameter target chamber with a TOF arm adjustable up to several meters in length. Timing signals are generated as the heavy ion passes through thin carbon foils, about 40 μg/cm, liberating electrons that are then accelerated to and collected on a channel plate. The time resolution obtained is about 300 psec.

To clearly separate chlorinelike ions, with $M \sim 35$, a mass resolution $M/\Delta M \sim 70$ is required. With a $1\frac{1}{2}$ m flight path, for an incident beam of 205 MeV ^{35}Cl, energy resolution of about 1% is needed. This was obtained using a large-solid-angle gas-ionization detector,[11] containing isobutane gas, with a stretched 100 μg/cm^2 polypropylene window with an area of 3200 mm^2. Z information was obtained from the counter as well. The solid angle was limited by the stop foil, only 314 mm^2 in area. Larger foils have problems with fragility and efficiency of electron collection. Thus, the effective solid angle was 0.08 msr. Because of the small solid angle, counting statistics for these runs were considerably poorer than for the telescope data. Cross sections were normalized using a monitor counter placed at 27°.

Event mode recording (EMR) was used to collect the time-of-flight data with 4096 channel resolution. Each Z region determined from the E_T-ΔE spectrum served as a gating condition in creating a mass spectrum for that specfic charge. An E_T vs $E_T(t-t_0)^2/k$ spectrum was generated where E_T is the sum of the anode signals from the gas ionization chamber, t is the TAC signal between the timing foils, and t_0 and k are constants that straighten the mass lines.

Energy spectra from completely separated mass groups (in contrast to the counter telescope experiment), ranging from ^{9}Be to ^{21}F, were obtained for the ^{16}O+^{232}Th reaction with a hybrid configuration of the TOF spectrometer. Timing was obtained using one carbon foil and a SSB detector placed in the back of the ionization chamber. Owing to incomplete charge collection in the SSB detector, a line of constant ΔE in the E_T-ΔE spectrum emanates from the elastic peak. This interferes with the energy spectra of oxygen isotopes with mass 16 or less and of nitrogen isotopes with mass 14 or less. Thus these products could not be measured. Otherwise this measurement included all transfer products with cross sections greater than 7 μb/sr.

For the measurement of ^{35}Cl+^{181}Ta at 205 MeV and $\theta_{lab}=70°$, carbon foils were used for both start and stop timing signals. Measured products included ^{29}Al to ^{38}Ar, although the mass spectrum in Fig. 2 only displays ^{29}Al to ^{36}S. Because of somewhat imprecise energy corrections due to losses in the entrance window that depend on mass as well as charge, the timing signal is used to calculate the energy in generating spectra rather than using the evaluated energy from the ionization detector.

III. DATA ANALYSIS AND RESULTS

A. ^{16}O+^{232}Th system

1. *Elastic scattering at 105 MeV*

An elastic scattering angular distribution was measured for the ^{16}O+^{232}Th system at 105 MeV. A thin 40 μg/cm^2 ^{232}Th target was used instead of the thick target in order to have a more precise energy determination, and the angular resolution of the telescope was limited to $\pm 0.1°$. The measurements were extended from $\theta_{lab}=30°$ to 110°, well forward and backward of the grazing angle. The elastic peak, whose width is consistent with the detector resolution of 1%, presumably includes inelastic excitation of the low-lying states in ^{232}Th as well.

An optical model fit was performed with the computer code JIB3,[12] assuming a Woods-Saxon form for the nuclear potential, with identical real

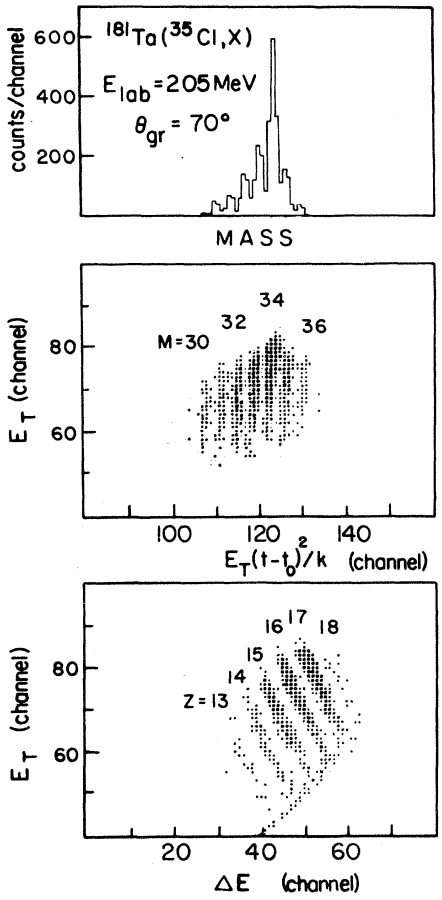

FIG. 2. Density plot of specific energy loss versus total energy (lowest panel), total energy versus mass (middle panel), and projection of this spectrum onto the mass axis (upper panel) for projectilelike products from the ^{35}Cl+^{181}Ta reaction at the grazing angle of 70° at 205 MeV incident energy.

and imaginary radii $R_0=r_0(A_1^{1/3}+A_2^{1/3})$ and surface diffuseness a. The Coulomb potential is for two uniformly charged spheres that touch at the Coulomb radius R_C. The program includes 99 partial waves and five adjustable parameters. The optical model fit obtained, with $\chi^2/N=1.6$, yields the following values of the parameters: $V=42.9$ MeV, $W=68.4$ MeV, $a=0.60$ fm, $r_0=1.2$ fm, and $r_{0_C}=1.2$ fm. The transmission coefficient attains a value of 0.5 for $l\simeq 42\hbar$, while the width of the smoothly varying region, determined by the values of l for which the transmission coefficient decreases from 0.9 to 0.1, is about $22\hbar$. The reaction cross section is 1.08 b.

The optical model fit is consistent with that done by Meyer *et al.*[13] for ^{20}Ne+^{235}U. Here, too, the ratio of the absorptive imaginary potential to the real potential depths is $W/V\sim 1.5$, reflecting the deformed character of the nucleus.

The distance of closest approach can be determined from the turning point of the grazing orbit, here defined as the Coulomb orbit with angular momentum $l_{1/2}$ for which the transmission coefficient equals 0.5. Referred to as the strong absorption radius, R_{SA}, it is evaluated as 12.6 fm. An interaction radius R_{int}, parametrized[14] from available elastic scattering data, often substitutes for R_{SA}. Since the value of R_{int} is within 1% of R_{SA} for ^{16}O+^{232}Th at 105 MeV, the parametrization is used to calculate the interaction radii of the other systems for which an elastic scattering analysis was not done.

The sharp cutoff approximation,[15] or quarter-point approach, is compared with the optical model analysis. From the data, $\theta_{1/4}=91°$. Therefore, $l_c=43\hbar$ and $R_{SA}=12.7$ fm, in agreement with the above results. The reaction cross section is evaluated as 0.88 b, low compared to the optical model value, because the gradual decrease of T_l about $l_{1/2}$ is markedly different from the sharp cutoff model, and the partial waves larger than $l_{1/2}$ included in the optical model analysis result in a larger reaction cross section.

2. *Optimal Q values*

The energy projections for the reaction products of the ^{16}O+^{232}Th grazing reaction at 105 MeV are shown in Fig. 3. The measured isotopes from the counter-telescope experiment include ^{9,10}Be, $^{11-13}$B, $^{12-15}$C, and $^{15-17}$N. The oxygen reaction products could not be separated accurately due to the presence of the dominant elastic channel. The beryllium isotopes have a slight high energy cutoff, as mentioned earlier. The TOF run, with complete mass separation albeit poorer statistics, measured isotopes with low yields, including ^{11,12}Be, ^{10}B, ^{16}C, ^{18}N, and $^{19-21}$F, as well as $^{16-20}$O. Of these, only ^{16}C and $^{16-19}$O have sufficient statistics to present meaningful energy projections and are included in Fig. 3. The spectral shapes and optimal energies of the products ^{9,10}Be, $^{11-13}$B, $^{12-15}$C, and $^{15-17}$N measured with TOF are in close agreement with those from the counter telescope run. The distributions in general are broad and asymmetric, spanning about 30–40 MeV and peaked at some optimal en-

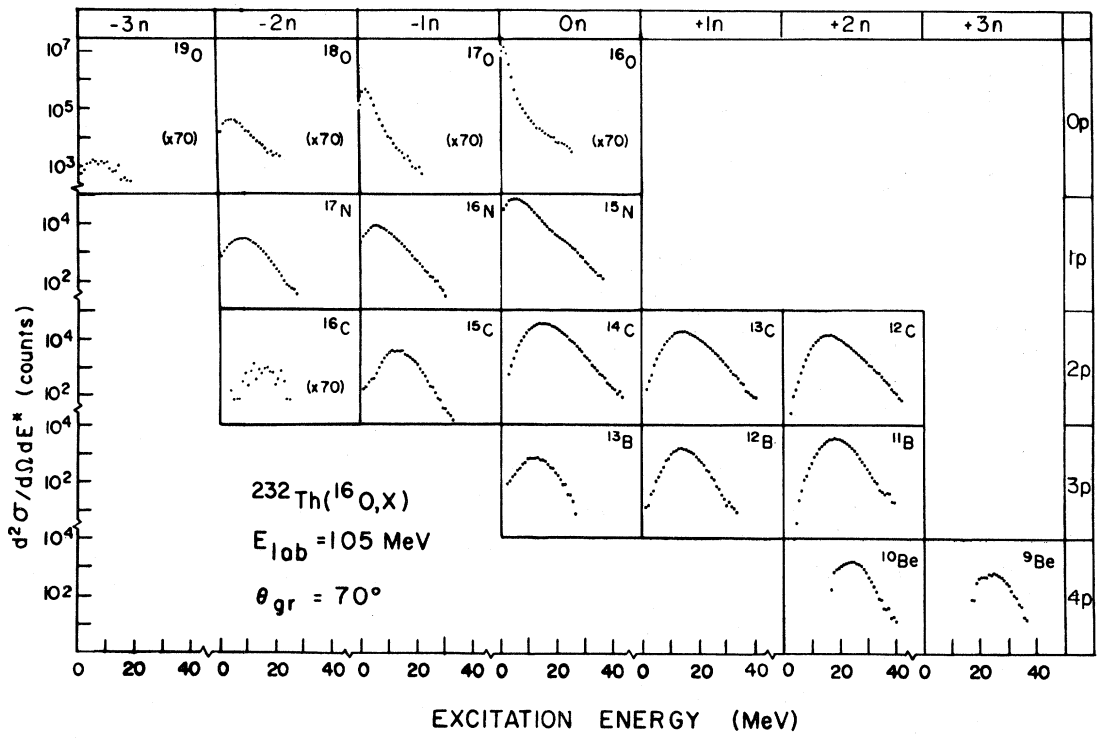

FIG. 3. Energy spectra of the projectilelike products from the $^{16}O+^{232}Th$ grazing reaction.

ergy. The spectral shape varies systematically with ΔN, the number of nucleons transferred, becoming less skewed as ΔN increases. The optimal energy is also strongly dependent on ΔN. Since the difference between the Coulomb energies of the entrance and exit channels, ΔE_C, is large, an effective Q value is defined to be the difference of the final and initial kinetic energies at the distance of closest approach, $Q^{\text{eff}}=\epsilon_f-\epsilon_i$. The effective optimal Q value can be written as $Q_{\text{opt}}^{\text{eff}}=Q_0-\langle E^*\rangle+\Delta E_C$, where the average value of the excitation energy $\langle E^*\rangle$ is the centroid of the experimental distribution. To compute the Coulomb energies, the interaction radius determined from the optical model fit is used, $R_{\text{int}}=12.6$ fm. Figure 4 shows $Q_{\text{opt}}^{\text{eff}}$ vs ΔN for the measured products of this reaction, where each symbol represents the isotopes of a given charge. In general, as ΔN increases, the energy dissipation smoothly approaches the fully relaxed limit, indicated by the arrow, where the ejectile is fully damped and is emitted with only the Coulomb repulsion energy. The energy loss appears to depend only on the number of transferred nucleons and not on the specific nature of the transferred nucleon (proton or neutron) or on the direction the nucleon travels, either from projectile to target or vice versa. For example, three-nucleon transfer includes ^{19}O $(-3n)$, ^{17}N $(1p,-2n)$, ^{15}C $(2p,-1n)$, ^{13}C $(2p,1n)$, and ^{13}B $(3p)$, all of which

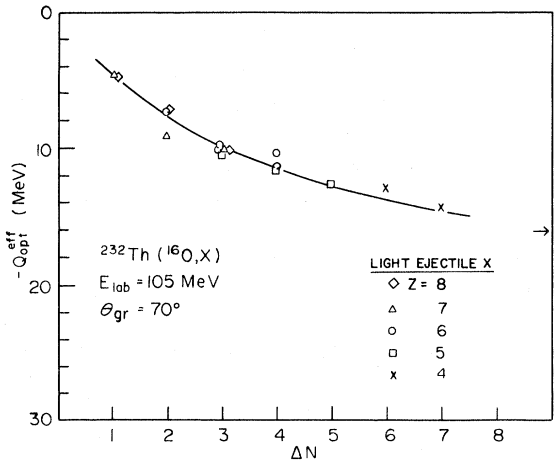

FIG. 4. Effective optimal Q value as a function of the number of transferred nucleons ΔN for the $^{16}O+^{232}Th$ grazing reaction.

have the same effective optimal Q value of about -10 MeV. Note that ^{15}C, ^{16}C, ^{16}N, and ^{17}N correspond to bidirectional transfer.

There have been several attempts to understand the optimal Q value based on simple classical and semiclassical considerations. One of the first, that of Buttle and Goldfarb,[16] is referred to as the orbit matching condition. An optimal grazing trajectory consists of an incident and final Rutherford orbit joined smoothly at the distance of closet approach, where nucleon exchange and energy loss are assumed to take place. This condition implies that transfer is most favorable when the orbits are matched. The calculated expression qualitatively describes the charge dependence of the optimal Q values but does not account for the mass dependence within a given charge, even after a recoil term is added to account for the different centers of mass of the incident and final channels.

A condition of velocity matching is conceivably another criterion for favorable transfer. Here the relative velocity v at the distance of closest approach is assumed to be the same immediately before and after transfer occurs. For systems with targets much heavier than projectiles, the velocity matching condition determines

$$Q_{\text{opt}}^{\text{eff}} = -\frac{\Delta N}{\mu_i}\epsilon_i \ .$$

Here ΔN is the net number of nucleons transferred, and μ_i is the reduced mass of the entrance channel.

The rate of energy damping is proportional to the available energy at the barrier, ϵ_i. A linear relation of $Q_{\text{opt}}^{\text{eff}}$ with ΔN is demonstrated by Mikumo *et al.*[17] for data ranging from ^{14}N+^{54}Cr at 64 MeV to ^{15}N+^{232}Th at 174 MeV. $Q_{\text{opt}}^{\text{eff}}$ saturates with respect to ΔN for $\Delta N \geq 4-5$, however, and the linear relation breaks down as the residual energy in the particle becomes insufficient to dissipate at the same rate for subsequent mass transfer.

There have been several efforts to explain the energy dissipation by statistical and macroscopic concepts such as friction and viscosity, because of the large number of degrees of freedom involved. A phenomenological approach is to use a classical velocity-proportional frictional force to describe the energy damping. Tsang[18] proposed a frictional force proportional to the volume integral of the product of the two nuclear density distributions and the relative velocity at each point. For a reaction near the grazing angle, the force is primarily tangential. Also, the range of partial waves contributing to the transfer reaction is very limited for the systems considered here, and the region of overlap of the nuclear surfaces can be considered to be constant for the participating partial waves. Thus, $F \simeq -kv$ where v is the relative velocity at the distance of closest approach during transfer. This leads[8] to an expression for the effective optimal Q value,

$$Q_{\text{opt}}^{\text{eff}} = -\left[1-\left[1-\frac{\Delta N}{\mu_i}\right]\exp\left[-\frac{\alpha}{\mu_i}\Delta N\right]\right]\epsilon_i \ . \tag{1}$$

The net number of transferred nucleons, ΔN, is known to be correlated with the amount of energy dissipated, which increases as the time of contact increases. Here, the simplest assumption is made, namely that the interaction time is proportional to the number of transferred nucleons, in order to arrive at Eq. (1).

The preceding model is applied to this reaction. The functional form of Eq. (1) is correct, since, for large ΔN, ϵ_f goes to zero and the asymptotic value of $Q_{\text{opt}}^{\text{eff}}$ is -16 MeV. The solid curve in Fig. 4 is a least-squares fit to the data obtained by varying the one parameter α, yielding $\alpha \simeq 4$. This simple model gives a good account of the data. The rate of energy damping depends on the damping coefficient, which is

$$\alpha/\mu_i = 0.27 \ .$$

3. *Relative cross sections*

Figure 5 shows $d\sigma/d\Omega$ as a function of ΔN, where again each symbol represents all isotopes of a given charge. The isotope yields for ^{10}B, ^{16}C, ^{18}N, $^{17-20}$O, and ^{19}F are taken from the TOF run. The product yields for ^{11,12}Be and ^{20,21}F have statistical errors larger than 30% and are not displayed. The logarithm of the cross section varies inversely with ΔN; moreover, the isotopes seem to fall along several lines, equally spaced and with constant slope. This trend may indicate that the reaction proceeds stepwise, each nucleon transfer having the same probability of occurrence whether a neutron or a proton transfer. The probabilities of some transfers are further diminished, dropping them to a lower line. For example, the cases of bidirectional nucleon exchange, including ^{16}N $(1p,-1n)$, ^{17}N $(1p,-2n)$ or ^{15}C $(2p,-1n)$, and ^{16}C $(2p,-2n)$, with $\Delta N = 2$, 3, and 4, respectively, are less favorable

than those cases which involve only stripping from the projectile, namely ^{14}C $(2p)$, ^{13}C $(2p,1n)$, and ^{12}C $(2p,2n)$. If one considers the reaction to proceed step by step, each intermediate projectilelike nucleus has four possibilities for single-nucleon transfer: neutron pickup or stripping and proton pickup or stripping. Energetically, the most favorable reaction is that with the largest (most positive) value of $Q_0+\Delta E_C$, where Q_0 is the ground state Q value and ΔE_C is the difference of the Coulomb energies before and after transfer. The path thus prescribed leads from the projectile ^{16}O to ^{15}N, then to ^{14}C, ^{13}C, ^{12}C, ^{11}B, ^{10}Be, and finally ^{9}Be; all of which lie along the top line. Note that the pairing energy accounts for successive proton or neutron transfers. An alternative path, also favorable, is $^{16}O \rightarrow ^{17}O \rightarrow ^{18}O$. Each step may also branch to less favorable transfers. For instance, ^{15}N can go to ^{16}N, which is less favorable energetically then ^{14}C, and, indeed, ^{16}N lies along the second line. In addition, ^{14}C might go to ^{15}C instead of ^{13}C, ^{13}C might go to ^{12}B, and so on. This simple procedure can in fact account for most of the observed isotopes in Fig. 5.

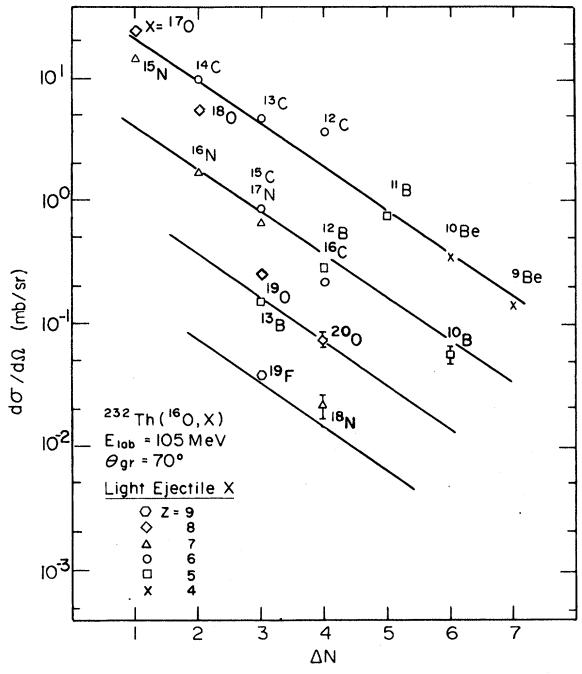

FIG. 5. Differential cross section at the grazing angle as a function of the number of transferred nucleons for the $^{16}O+^{232}Th$ reaction. The lines indicate various branches, as described in the text, but are not fitted to the data.

In summary, the relative probability of each exit channel of the transfer reaction can be empirically expressed as

$$p(\Delta N)=p(1)\exp\{\gamma[\Delta N+2(l-1)]\}\ . \quad (2)$$

Here, the probability $p(1)$ for one-nucleon transfer is about 0.3, and the average slope $\gamma=-0.8$. The line $(l=1,2,3\ldots)$ along which a given isotope falls appears to depend on how favorable energetically the transfer of a given nucleon—proton or neutron—is at each step.

The ^{12}C $(2p,2n)$ exit channel deviates somewhat from the systematics, having a cross section close to that expected for three-nucleon transfer rather than for four-nucleon transfer. This is probably because the two protons and two neutrons cluster part of the time as an alpha particle, making transfer more probable. Two component transfers are discussed in Sec. IV B.

It is of interest to compare these systematics with those of Artukh *et al.*[4] where the yields for the isotopes of each charge depend exponentially (to within a factor of 2) on (Q_0),

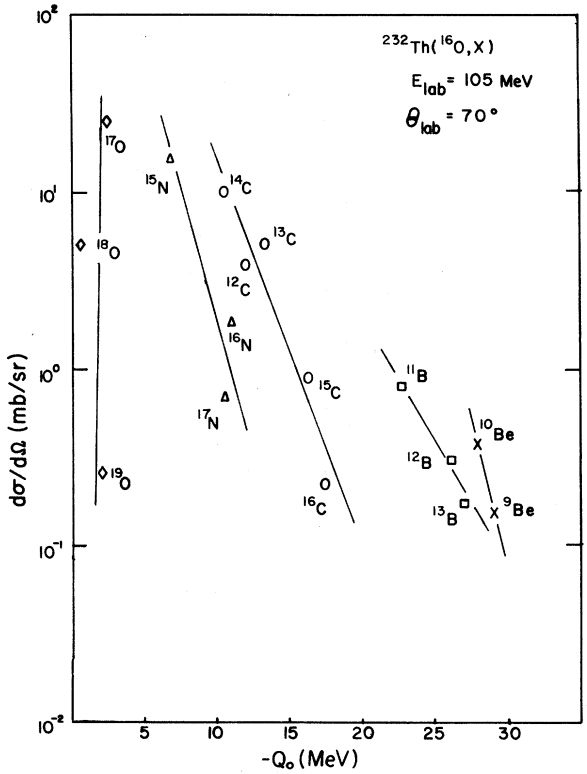

FIG. 6. Differential cross section for the various projectilelike products of the $^{16}O+^{232}Th$ reaction at the grazing angle of 70° and 105 MeV bombarding energy displayed as a function of the ground state to ground state Q value Q_0. The lines are merely to guide the eye.

$\sigma \sim \exp[(Q_0+\Delta E_C)/T]$. Bondorf *et al.*[5] explain this trend on Q_0 to be a consequence of partial statistical equilibrium at a temperature T. A Coulomb correction term ΔE_C is added to Q_0 to qualitatively explain the differences among the lines for each charge. It should be noted that Lee and Braun-Munzinger[6] derive the same expression for the cross section by assuming that nucleons are transferred successively with a probability P and that each step is well matched kinematically. The parameter T is related to the mean energy transfer and the probability of transfer, and not to the temperature. In Fig. 6 the yields are displayed versus Q_0. It is seen that the exponential dependence on Q_0 is roughly observed. Yet, large deviations are present and the slopes which should be the same, depending only on T, are quite different for the different elements. The observed systematics with ΔN described above give a far better description of the data in this regime, with bombarding energies nearer the Coulomb barrier than in the measurements of Artukh *et al.*[4]

4. *Angular distribution at 105 MeV*

Angular distributions of the $^{16}O+^{232}Th$ reaction at 105 MeV were measured for the transfer products ^{10}Be, ^{11}B, ^{12}C, ^{13}C, ^{14}C, and ^{15}N. All exhibit broad bell-shaped distributions with a maximum near $\theta_{lab}=70°$ as seen in Fig. 7. Other isotopes were observed at all angles, but their yields relative to the dominant isotopes of that charge were too small to extract accurate cross sections at all angles. The

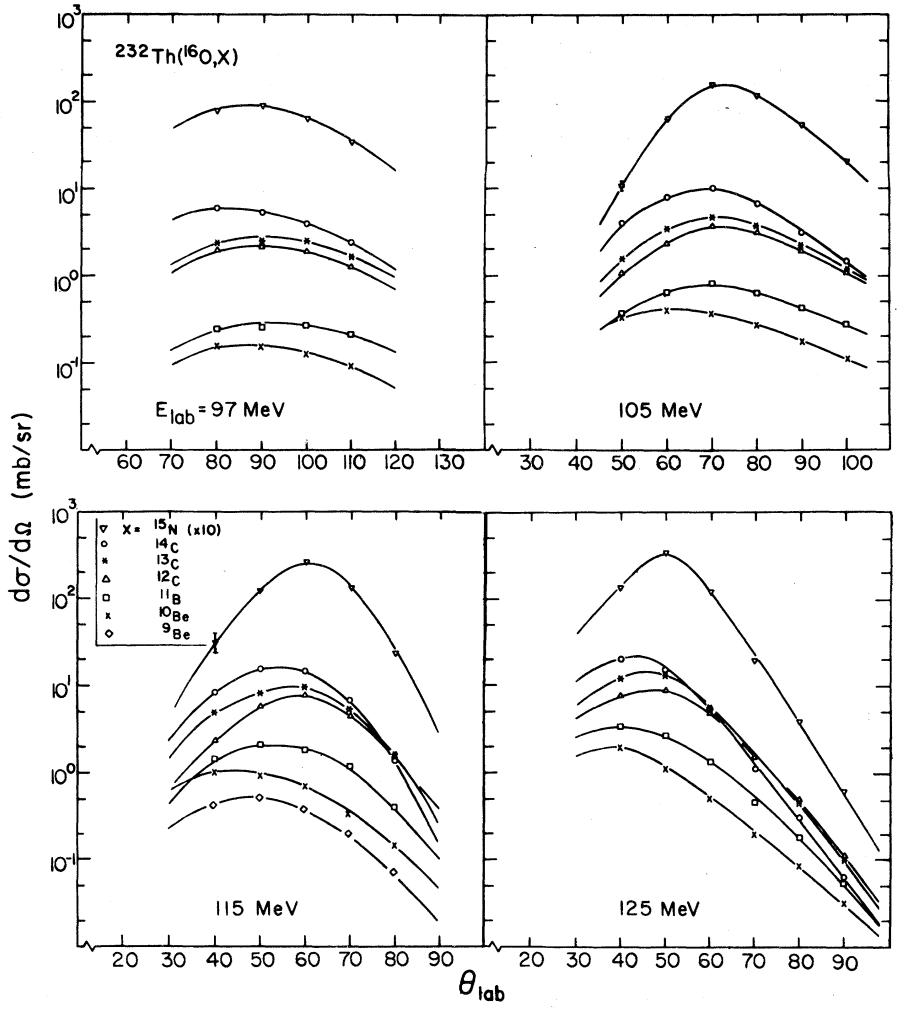

FIG. 7. Angular distributions for the projectilelike products from the $^{16}O+^{232}Th$ grazing reaction at 97, 105, 115, and 125 MeV bombarding energy.

solid curves are drawn through the measured values to guide the eye. The cross sections were normalized with Rutherford scattering in the monitor detector. At the grazing angle, the transfer cross section $(d\sigma/d\Omega)_T=71$ mb/sr. This includes the transfer cross section from all Be, B, C, N, and O isotopes, except for the inelastic ^{16}O cross section, which is not separable from the elastic cross section. Even though the measured values of θ do not extend from 0° to 180°, the unmeasured cross section is only a small fraction of the total. The total angle integrated cross section, then, is 225 ± 20 mb. This transfer cross section is about 20% of the reaction cross section of 1.08 b. (The rest of the reaction cross section presumably goes into fusion followed by fission.)

The angular distributions change gradually from one-nucleon to six-nucleon transfer, becoming broader and slightly more forward peaked. This suggests an increase in the mean interaction time with increasing nucleon transfer. The dependence of the broadening of the angular distributions with time is not actually known. However, it is seen in Fig. 8 that the variance of the distribution is linear with respect to ΔN. The ^{12}C exit channel, a $(2p,2n)$ transfer, deviates considerably from this relationship. This may well be due to a large probability for the transfer of a cluster (α particle) as well as four distinct nucleons. The variance of the angular distribution, the optimal Q value, and relative cross section for the ^{12}C channel are all consistent with the transfer of an α cluster occurring $\frac{1}{3}$ of the time. The "X" in Fig. 8 signifies the variance of a four-particle transfer, assuming the measured variance of ^{12}C includes the influence of α transfer $\frac{1}{3}$ of the time.

The energy spectra at different scattering angles were analyzed to study the dependences of spectral shape and optimal Q value on angle. The data for $\theta_{lab}=50°-100°$ have been analyzed for the transfer products ^{11}B, ^{12}C, ^{13}C, ^{14}C, and ^{15}N. It is found that the energy loss is minimal for the most peripheral collisions at the grazing angle near $\theta_{lab}=70°$ for few-nucleon transfer and near $\theta_{lab}=60°$ for many-nucleon transfer. Scattering forward and backward of the grazing angle is more strongly damped. The rate of energy damping as a function of ΔN is shown in Fig. 9 for four different scattering angles. Collisions that scatter backward of the grazing angle damp stronger with respect to nucleon transfer, although the fully relaxed limit is apparently the same, implying similar deformations in the exit channel. The solid curves drawn are ob-

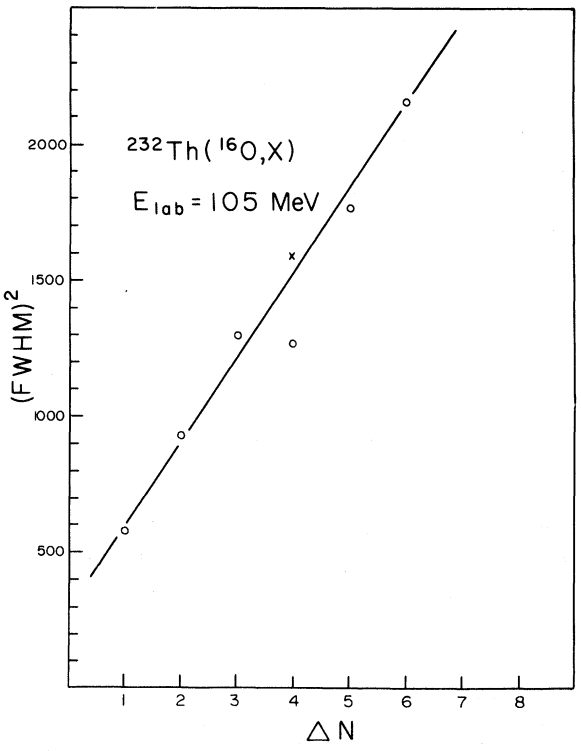

FIG. 8. Variance of the angular distributions shown in Fig. 7 as a function of the number of transferred nucleons ΔN. The X indicates the variance for the four-nucleon component if one assumes that $\frac{1}{3}$ of the transfers are the cluster type, with a variance corresponding to $\Delta N=1$.

tained from the damping model with $\alpha/\mu_i=0.27$ for $\theta_{lab}=70°$, as stated before, and $\alpha/\mu_i=0.54$ for $\theta_{lab}=100°$. The larger damping coefficient implies a larger region of overlap of the nuclear surfaces for a nongrazing collision. It is not clear, though, whether radial friction should be taken into account. It appears that the form of Eq. (1) describes the average energy loss for nongrazing reactions if the damping coefficient increases as θ increases.

5. *Bombarding energy dependence*

The $^{16}O+^{232}Th$ reaction was studied at various bombarding energies, from 90 MeV, near the Coulomb barrier, to 125 MeV. The energy distributions for the grazing reactions become noticeably broader as the incident energy increases above the Coulomb barrier, whose value imposes a cutoff at high excitation energy corresponding to a fully re-

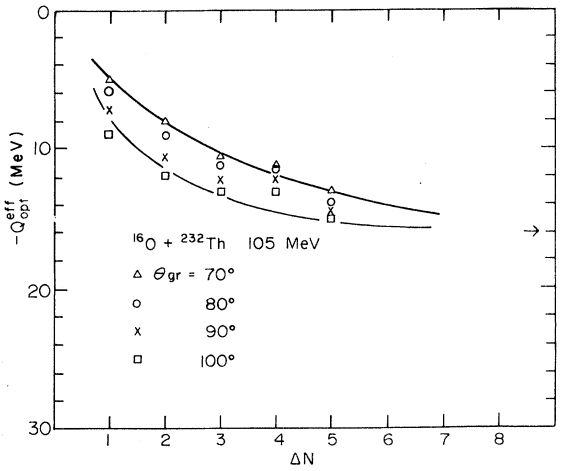

FIG. 9. Effective optimal Q value as a function of the number of transferred nucleons, ΔN, for various scattering angles, for the $^{16}O+^{232}Th$ reaction.

laxed collision.

The average excitation energy also increases with bombarding energy. In fact, the dependence of Q_{opt}^{eff} with ΔN is seen in Fig. 10 to be very similar for the different energies, although as the available energy above the barrier increases, the asymptotic value of Q_{opt}^{eff} decreases. The data shown are for the grazing reactions; $\theta_{gr}=80°$ at $E_{lab}=97$ MeV, 70° at 105 MeV, 60° at 115 MeV, and 50° at 125 MeV. The interaction radius has been found to be nearly independent of projectile energy—perhaps decreasing very slightly with increasing energy—for measure-

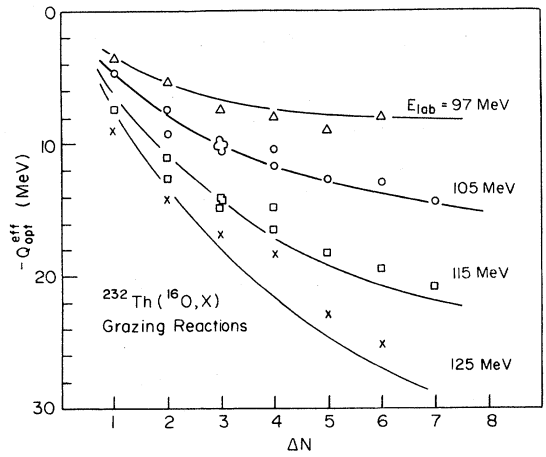

FIG. 10. Effective optimal Q value as a function of the number of transferred nucleons for the $^{16}O+^{232}Th$ grazing reaction at various bombarding energies.

ments of $^{16}O+^{208}Pb$ by Videbaek *et al.*[19] and $^{20}Ne+^{235}U$ by Meyer *et al.*[13] Therefore, the value $R_{int}=12.6$ fm determined for $^{16}O+^{232}Th$ at 105 MeV is used to evaluate Q_{opt}^{eff} at the other incident energies. Consequently this implies the degree of overlap of the nuclear surfaces during a grazing collision remains constant as the projectile energy increases. However, one might expect the mean interaction time to be inversely proportional to the relative velocity during transfer. If the damping constant is inversely weighted by the average velocity at the distance of closest approach, then $\alpha/\mu_i=0.44$, 0.27, 0.20, 0.17 for $E_{lab}=97$, 105, 115, and 125 MeV, respectively. The solid curves in Fig. 10 are obtained by using these values of the damping constant. The model accounts well for the data, although at 125 MeV the energy loss is overestimated for large ΔN. This implies that the rate of energy damping does not remain constant at higher energies as ΔN increases.

The isotope yield dependence as a function of ΔN is studied for different bombarding energies in Fig. 11. Here only the dominant chain, ^{15}N-^{14}C-^{13}C-^{12}C-^{11}B-^{10}Be-^{9}Be, is shown for clarity. Again the measurements are at the grazing angle. The logarithm of the cross section is a linear function of ΔN at all energies, although the rate changes at which the cross section decreases with increasing ΔN. This is demonstrated by passing a least-squares line through the data to determine the average slope γ in Eq. (2). The values of the average slope are plotted as a function of E_{lab} in Fig. 12. The absolute value of γ monotonically decreases as the bombarding energy increases. In other words, at higher energies the probability of many-nucleon transfer increases relative to few-nucleon transfer.

The systematics also change with scattering angle as illustrated in Fig. 13 for $E_{lab}=105$ MeV. Again a least-squares fit is performed to determine the average slopes, whose values are plotted as a function of θ_{lab} in Fig. 12. The most peripheral collision, at $\theta_{gr}=70°$, favors the few-nucleon transfer to a greater degree than more deeply penetrating collisions. The relative probability for one-nucleon transfer to ^{15}N distinctly drops at $\theta_{lab}=50°$ and 60°, and in general the logarithmic trend of $(d\sigma/d\Omega)$ with ΔN tends to level out for scattering both forward and backward of the grazing angle.

The angular distributions were measured for $^{16}O+^{232}Th$ at $E_{lab}=97$, 115, and 125 MeV as well as at 105 MeV. Figure 7 shows that the distributions shift forward and become narrower as the incident energy increases. At the grazing angle, the

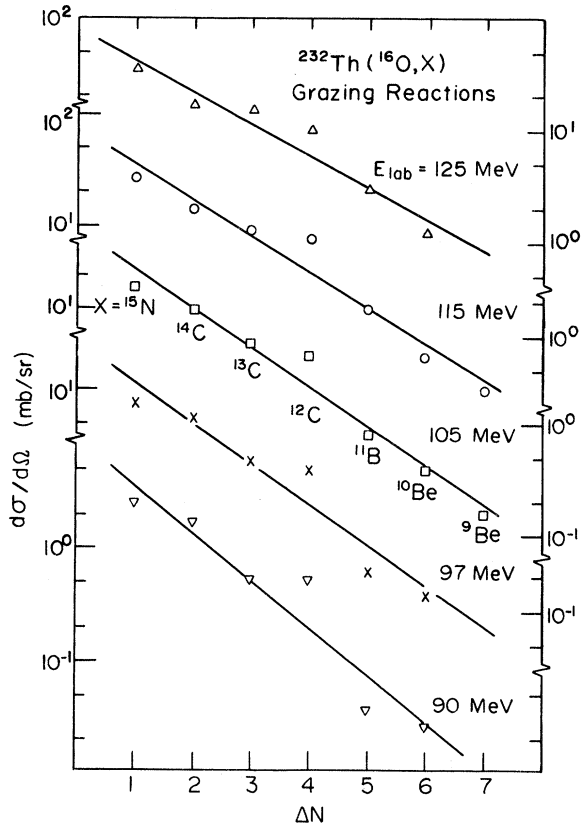

FIG. 11. Differential cross section as a function of the number of transferred nucleons for the $^{16}O+^{232}Th$ grazing reaction at various bombarding energies. The lines indicate least-squares fits to Eq. (2).

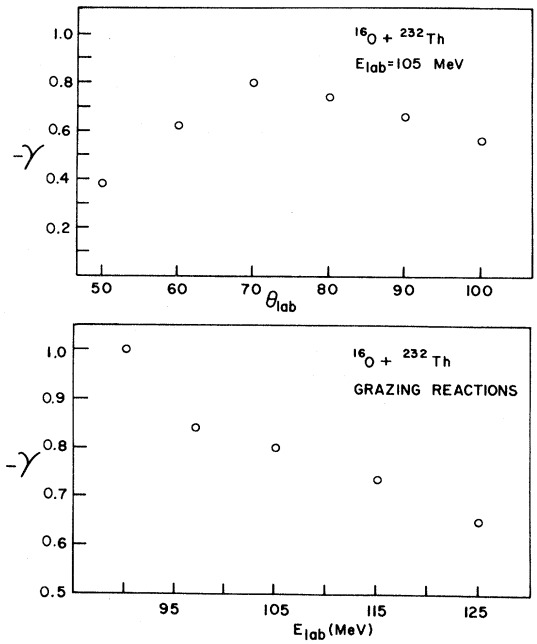

FIG. 12. Average slope of differential cross sections as a function of laboratory energy at the grazing angle (bottom frame) and as a function of scattering angle at a fixed incident energy of 105 MeV (top frame) for the $^{16}O+^{232}Th$ reaction.

differential cross section for these six products, which constitutes about 90% of the cross section for all Be, B, C, and N isotopes, increases from about 5 mb/sr at 90 MeV to 95 mb/sr at 125 MeV. The angular distributions for 115 MeV are integrated to yield $\sigma_T \simeq 154$ mb. This is 35% higher than the corresponding yield of 113 mb at 105 MeV. The angular distributions for $E_{lab}=97$ and 125 MeV, though incomplete, are also integrated, including extrapolated values of the cross section extending 10° further than the measured values. Although measurements at small angles are missing, particularly at 125 MeV, these would not contribute very much to the cross section due to the $\sin\theta$ factor. At 97 MeV the summed cross section σ_T for these products is 84 mb, and at 125 MeV σ_T is 170 mb. These numbers have uncertainties of about 15%, not including the missing cross section of transfer of ^{17}O and ^{18}O, which was measured to be about one-half of the total transfer cross section for $E_{lab}=105$ MeV. Videbaek *et al.*[19] measured transfer cross sections for $^{16}O+^{208}Pb$ and $^{16}O+^{181}Ta$. For $^{16}O+^{208}Pb$, at $E_{lab}=83-102$ MeV, the oxygen transfer cross section also contributes about one-half of the total; whereas for $^{16}O+^{181}Ta$, at $E_{lab}=83-96$ MeV, oxygen contributes only one-fourth.

Figure 14 shows the transfer cross sections for each of the six products increasing as a function of E_{lab}/E_C more rapidly for multinucleon transfer. Also shown are the summed cross sections for comparison with those of the $^{16}O+^{208}Pb$ and $^{16}O+^{181}Ta$ measurements, excluding oxygen cross sections. The values of $E_C=88$, 83.4, and 76.9 MeV, calculated with the interaction radius, are used for $^{16}O+^{232}Th$, ^{208}Pb, and ^{181}Ta, respectively.

Figure 15 shows the cross-section systematics as a function of angle for $E_{lab}=125$ MeV. As in Fig. 13 for $E_{lab}=105$ MeV, the logarithmic dependence of $d\sigma/d\Omega$ with ΔN tends to level out for scattering reactions other than at the grazing angle, which is especially noticeable for the most backward angles. In addition, the systematic dependence is not quite as monotonic at these backward angles; in fact it peaks at the ^{12}C exit channel.

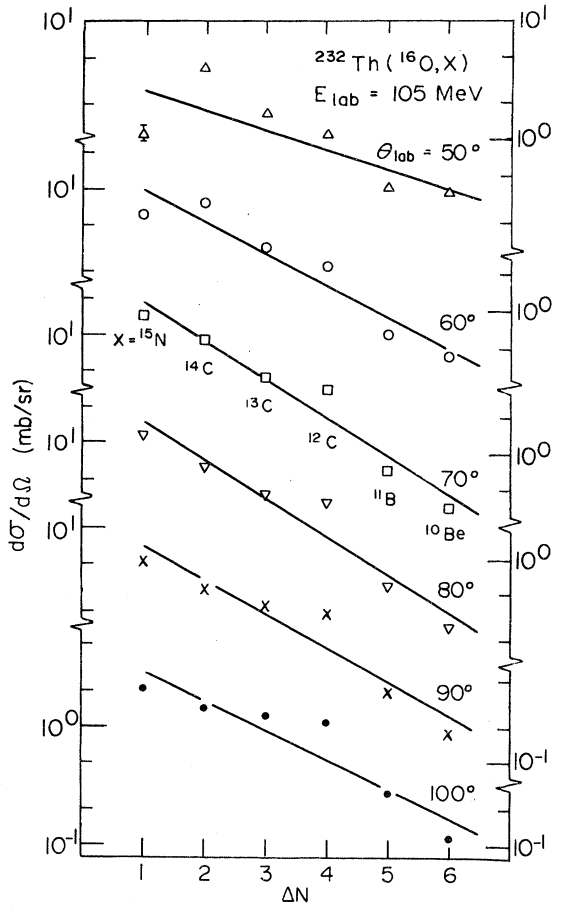

FIG. 13. Differential cross section for the projectile-like products as a function of the number of transferred nucleons for various scattering angles about the grazing angle for the $^{16}O+^{232}Th$ reaction.

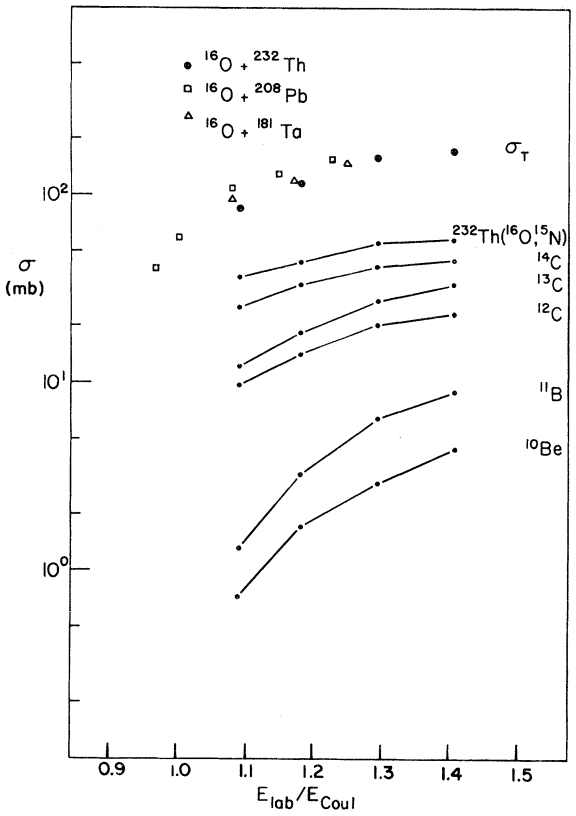

FIG. 14. Integrated cross sections for the various transfer groups and for the sum of all the groups (marked σ_T) for the $^{16}O+^{232}Th$ reaction (solid dots) as a function of the incident energy relative to the Coulomb barrier. These data for σ_T are compared with the $^{16}O+^{208}Pb$ and $^{16}O+^{181}Ta$ data for σ_T given in Ref. 19.

B. Other systems

1. $^{15}N+^{232}Th$

The projectile dependence of these trends is investigated by substituting a nitrogen beam for oxygen. The $^{15}N+^{232}Th$ reaction was measured at a bombarding energy of 95 MeV which approximately matches the incident velocity at the distance of closest approach, about $0.05c$, with the $^{15}O+^{232}Th$ reaction at 105 MeV. The $^{15-18}N$ channels were not well separated from the elastic channel. A qualitative comparison with $^{16}O+^{232}Th$ indicates similarities in the spectral shape for the same transfer reactions. All comparisons of spectral shapes, optimal Q values, and isotope yields between these two systems are for identical transfer reactions and not final products: for example, the one-proton transfer ($^{16}O,^{15}N$) and ($^{15}N,^{14}C$).

Nitrogen was bombarded on thorium at energies of 86 and 103 MeV as well, to match the oxygen reactions at 97 and 115 MeV. Again the spectra broaden as E_{lab} increases and gradually become symmetric as ΔN increases. The average excitation energy increases, as well, for larger E_{lab} and ΔN. In Fig. 16 the effective optimal Q values are plotted as a function of ΔN for these three energies, displaying the same dependence as the $^{16}O+^{232}Th$ reaction. In fact, the values of Q_{opt}^{eff} are nearly identical for the two systems, demonstrating that the energy damping depends primarily on the number of nucleons transferred and not on the nuclear structure of the interacting particles of these systems. To evaluate Q_{opt}^{eff} the interaction radius is taken as 12.6 fm, the measured value for $^{16}O+^{232}Th$. The solid curves in

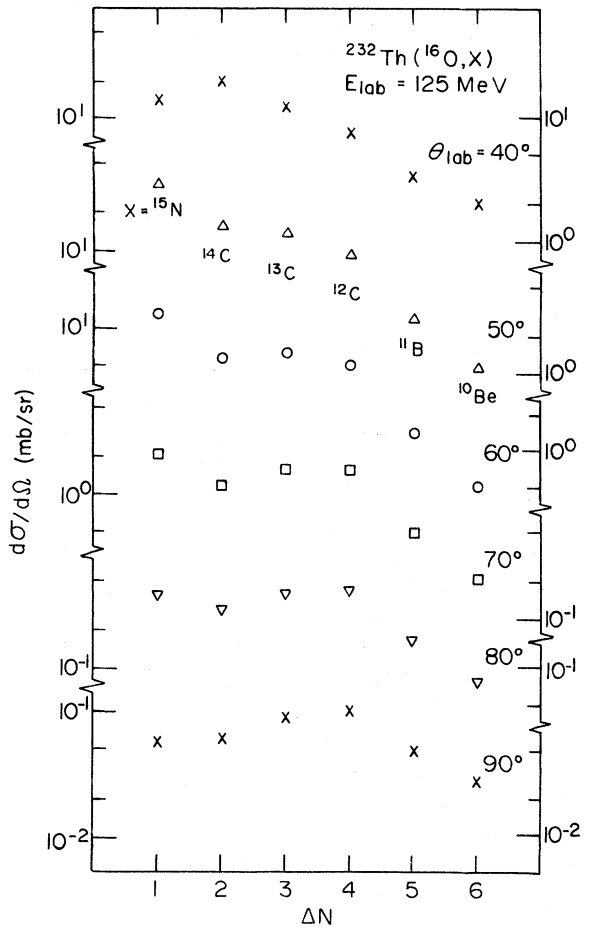

FIG. 15. Differential cross section of the projectile-like products as a function of ΔN at various scattering angles about the grazing angle for the $^{16}O+^{232}Th$ reaction at 125 MeV.

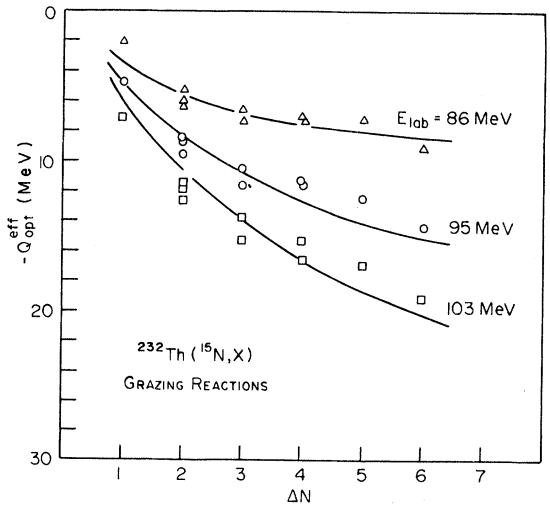

FIG. 16. Effective optimal Q value as a function of the number of transferred nucleons ΔN for the $^{15}N+^{232}Th$ reaction at the grazing angle for various incident energies. The curves show the expected dependence as given by Eq. (1).

Fig. 16 are obtained in the same manner as before with the damping model. The constant damping coefficients of $\alpha/\mu_i=0.42$, 0.25, and 0.20, for $E_{lab}=86$, 95, and 103 MeV, respectively, are used. The small differences between these values and those used for $^{16}O+^{232}Th$ take into account the slightly mismatched velocities of the two systems.

The systematics of the differential cross section with ΔN for $^{15}N+^{232}Th$, shown in Fig. 17, can also be compared with the results for $^{16}O+^{232}Th$. Here, the logarithmic dependence of $d\sigma/d\Omega$ as a function of ΔN is even more striking for these grazing reactions at the three bombarding energies. For example, the $(2p,2n)$ transfer $^{232}Th(^{15}N,^{11}B)$ is slightly deviant, but much less so than the $(2p,2n)$ transfer $^{232}Th(^{16}O,^{12}C)$. This implies that an alpha particle is more likely to form in the transfer from a four-alpha cluster ^{16}O to a three-alpha cluster ^{12}C. Here, the same procedure of considering the energetics dicates the favorable isotopes along the dominant chain: ^{15}N-^{14}C-^{13}C-^{12}C-^{11}B-^{10}Be-^{9}Be, the same progression as before. The probability is very similar for the two reactions. The average slopes in Fig. 18 have the values $\gamma=-0.89$, -0.80, and -0.76, for $E_{lab}=86$, 95, and 103 MeV, respectively, which are close to those values for the oxygen data ($\gamma=-0.84$, -0.80, and -0.74 for $E_{lab}=97$, 105, and 115 MeV).

Measurements about the grazing angle were taken for $^{15}N+^{232}Th$, ranging from $\theta_{lab}=60°-90°$ at 95 MeV and from $50°-80°$ at 103 MeV. The angular distributions peak near 70° at 95 MeV and near 60° at 103 MeV. Again, data at forward angles are lacking; still, the distributions are integrated to yield values of σ_T with uncertainties of about 15%. These values do not include isotopes of nitrogen. Therefore, σ_T probably represents about one-half of the total transfer cross section. The values of $\sigma_T=93$ and 121 mb, for 95 and 103 MeV, respectively, are about 80% of the corresponding transfer cross sections σ_T for $^{16}O+^{232}Th$ at 105 and 115 MeV.

The scattering angle dependence of $\ln(d\sigma/d\Omega)$ with ΔN for $^{15}N+^{232}Th$ at $E_{lab}=95$ and 103 MeV is also studied. The features are the same as for

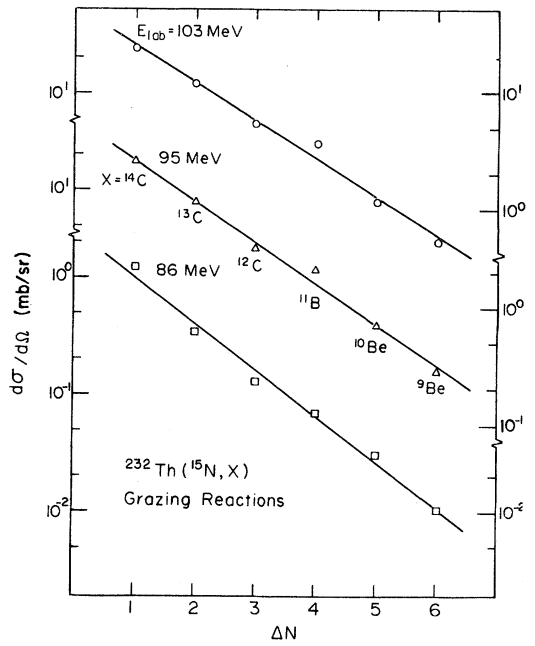

FIG. 17. Differential cross section for projectilelike products scattered at the grazing angle as a function of the number of transferred nucleons ΔN for the $^{15}N+^{232}Th$ reaction at three incident energies 86, 95, and 105 MeV. The lines are least-square fits. The deviation from the line for $\Delta N=4$, due to the four nucleon cluster transfer, increases with increasing incident energy.

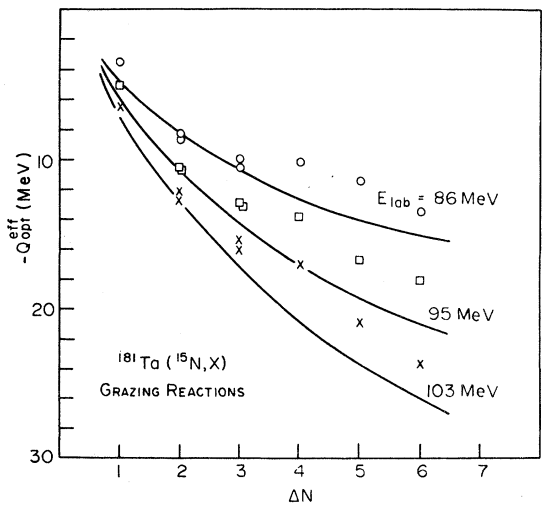

FIG. 18. Effective optimal Q values as a function of the number of transferred nucleons ΔN for the $^{15}N+^{181}Ta$ reaction at the grazing angle and at three incident energies 86, 95, and 103 MeV. The curves show the expected dependence given by Eq. (1).

$^{16}O+^{232}Th$; at increasing angles back of grazing, the average slope becomes less severe as many-nucleon transfer increases in probability relative to few-nucleon transfer.

2. $^{15}N+^{181}Ta$

Nitrogen bombardment on tantalum was investigated to see the effects, if any, of using a lighter target. The grazing reaction was measured for an incident energy of 86 MeV, which approximately matches $^{15}N+^{232}Th$ at 95 MeV and $^{16}O+^{232}Th$ at 105 MeV. The general features of the energy spectra are the same, the most noticable difference being the presence of a peak for $(1p)$ transfer at about 4 MeV, in addition to the usual optimal energy peak. The same peak appears at 4 MeV for the reactions at 95 and 103 MeV and is probably due to an excited state in the heavy nucleus ^{182}W.

The optimal Q values, as a function of ΔN, are presented in Fig. 18. The solid curves are obtained from the damping model, using damping coefficients of $\alpha/\mu_i=0.25$, 0.19, and 0.17, for $E_{lab}=86$, 95, and 103 MeV, respectively. Again the small differences between these values and those for the corresponding reactions of $^{16}O+^{232}Th$ at $E_{lab}=105$, 115, and 125 MeV account for the slightly mismatched velocities. For $^{15}N+^{181}Ta$, the parametrized interaction radius gives a value $R_{int}=11.85$ fm. This value of R_{int} determines a Coulomb barrier which causes the model to overestimate the energy loss for large ΔN, as seen in Fig. 18.

The angular distribution at 95 MeV was measured in a range of $\theta_{lab}=40°-70°$. The general features are similar for the lighter tantalum target and the heavier thorium target. The cross sections at 86 and 95 MeV are very similar to those of the corresponding reactions of $^{15}N+^{232}Th$ at 95 and 103 MeV, respectively. The grazing peaks differ by about 10° for the two systems. The integrated cross section of 110 mb at 95 MeV is about 90% of the value for $^{15}N+^{232}Th$ at 103 MeV.

3. $^{35}Cl+^{181}Ta$

Figure 19 displays the energy spectra for $^{35}Cl+^{181}Ta$. Despite the poor statistics, the data demonstrate the same general features of the transfer reactions with lighter projectiles. For ex-

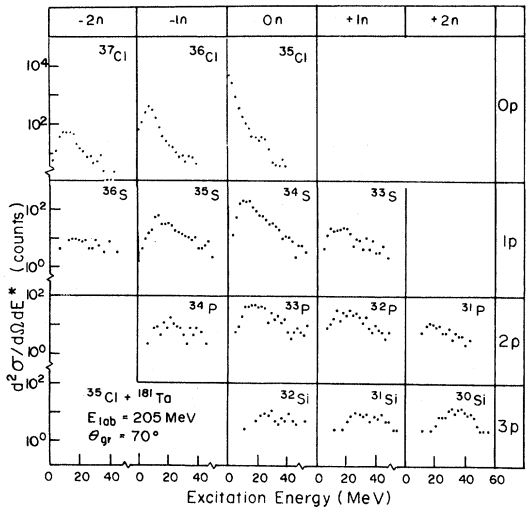

FIG. 19. Energy spectra for projectilelike particles scattered at the grazing angle for the $^{35}Cl+^{181}Ta$ reaction at 205 MeV. The incident energy was chosen to have the same grazing angle as the $^{16}O+^{232}Th$ reaction at 105 MeV.

ample, one-nucleon transfer, $(1p)$ to ^{34}S and $(-1n)$ to ^{36}Cl, are again the dominant exit channels with asymmetric energy spectra. The incident velocity at the distance of closest approach for $^{35}Cl+^{181}Ta$ at 205 MeV is matched to that of $^{16}O+^{232}Th$ at 105 MeV. An interaction radius of 12.73 fm is used here. The effective optimal Q values are plotted as a function of ΔN in Fig. 20 and show the familiar dependence, although the scatter of the experimental values is large, due to the low counting statistics. The solid line demonstrates the fit obtained with the same damping constant used for the $^{16}O+^{232}Th$ data, $\alpha/\mu_i=0.27$. Despite the uncertainty, the fit clearly accounts well for the average values. This implies that for both reactions, at similar velocities, the relative rate of energy damping is the same, even though chlorine is twice as large as oxygen and has a different structure. It also implies that the region of overlap of the surfaces of the two colliding nuclei is similar for both grazing reactions.

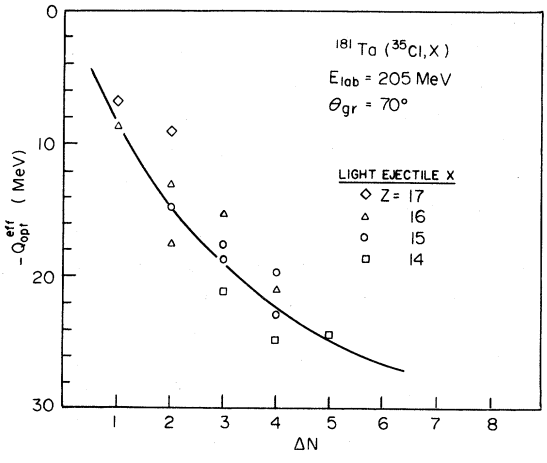

FIG. 20. Effective optimal Q value as a function of the number of transferred nucleons ΔN for the $^{35}Cl+^{181}Ta$ reaction at the grazing angle. The curve shows the expected dependence given by Eq. (1).

At $\theta_{lab}=70°$, the transfer cross section is determined to be 122 mb/sr, including chlorine isotopes. The cross-section dependence upon ΔN is compared in Fig. 21 with the corresponding reactions of $^{16}O+^{232}Th$, $^{15}N+^{232}Th$ and $^{15}N+^{181}Ta$. The dominant chain in the $^{35}Cl+^{181}Ta$ reaction, ^{34}S-^{33}P-^{32}P-^{31}P-^{30}Si-^{29}Al, has nearly the same logarithmic decrease of $d\sigma/d\Omega$ with ΔN as the other reactions. The average slope $\gamma=-0.71$ for this reaction compares with $\gamma=-0.80$ for both $^{16}O+^{232}Th$ and $^{15}N+^{232}Th$ and with $\gamma=-0.87$ for $^{15}N+^{181}Ta$.

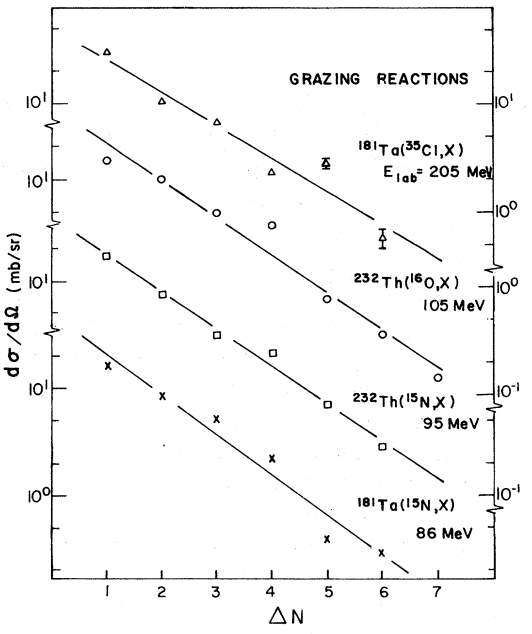

FIG. 21. A comparison of the differential cross sections at the grazing angle as a function of transferred nucleons ΔN for four different reactions, as indicated. The lines show the similarity of slope for these four reactions.

IV. SURPRISAL ANALYSIS

A. Introduction

The discussion of heavy-ion transfer reactions in terms of a statistical approach follows from a generalization of the maximal entropy formalism to collision processes.[20] The principal of maximum entropy[21] states that the most probable macrostate of a system is the one for which the entropy is a maximum, subject to the constraints that characterize the system. The procedure for finding a constrained maximum of the entropy has been described in detail elsewhere,[8] so only a brief summary is presented here.

The experimental distribution (p_i) is compared with the prior or statistical distribution (p_i^0). This distribution, with entropy S_0, is the one for which the available phase space would be uniformly populated, as is found in the absence of constraints. The information content is defined as $\Delta S = S_0 - S = \sum_i p_i \ln(p_i/p_i^0)$. Maximizing the entropy S is equivalent to minimizing the information content. This determines the distribution of maximal entropy to be

$$p_i^{\mathrm{ME}} = p_i^0 \exp\left[-\lambda_0 - \sum_{r=1}^{m} \lambda_r A_r(i)\right] . \tag{3}$$

The observable quantities A_r determine the m constraints, $\langle A_r \rangle = \sum_i p_i A_r(i)$. The distribution of maximum entropy (p_i^{ME}) is determined by a computer routine written by Alhassid *et al.*,[22] which solves for the Lagrange parameters λ_r.

The surprisal I measures the deviation of the observed distribution from the statistical distribution, $I = -\ln(p_i/p_i^0)$. For the distribution of maximal entropy, $I = \lambda_0 + \sum_r \lambda_r A_r(i)$; thus, the surprisal is a linear combination of the observable quantities A_r. It is important to realize that the principle of maximum entropy cannot predict with certainty what will happen in a real experiment. Nevertheless, the probability distribution given in Eq. (3) is overwhelmingly the most likely one to be observed, provided, of course, that the physical constraints assumed in the calculation are those that truly exert an influence on the outcome of the experiment. In short, the predicted probabilities describe the state of knowledge based on the available information.

The prior distribution or available phase space, with which the experimental distribution is compared, is given by a product of the internal nuclear level density ρ_J and the translational level density ρ_T. Thus

$$p_i^0 = \rho^0(E) = \rho_J(E^*)\rho_T(E_f) ,$$

where E^* is the internal or excitation energy and E_f is the translational or kinetic energy. Owing to the high degeneracy of nuclear states for thoriumlike nuclei at excitation energies $\gtrsim 1$ MeV, the nucleus can be treated as a fully degenerate gas of independent fermions moving in an average potential. The average internal level density is the number of ways the excitation energy can be distributed among the single-particle levels. For a Fermi gas with equal number of neutrons and protons and with total angular momentum J,[23]

$$\rho_J(E^*) \sim (2J+1)U^{-2}\exp 2(aU)^{1/2} , \tag{4}$$

where $U = E^* - E_{\mathrm{rot}} - E_{\mathrm{PE}}$. The rotational energy E_{rot} is given by

$$E_{\mathrm{rot}} = J(J+1)\hbar^2/2I_{\mathrm{rig}} .$$

An average pairing energy correction, included to account for excitation energy that goes into breaking neutron or proton pairs, is expressed[23] as $E_{\mathrm{PE}} = 12\delta A^{-1/2}$ MeV, where $\delta = 0$ (odd-odd), 1 (odd-even), or 2 (even-even).

The internal level density should actually be a product of the level densities of both nuclei. For an asymmetric system such as $^{16}\mathrm{O}+^{232}\mathrm{Th}$, however, the level density of the heavy dominates that of the light nucleus.

Since the surprisal analysis of the energy spectra in transfer reactions depends strongly on the functional form of the prior distribution, it is important to ascertain the validity of the expression in Eq. (4). The formula, based on Bethe's original calculation, makes use of the continuous approximation, which assumes equidistant single-particle level spacing rather than the proper single-particle level density of a Fermi gas, which depends on the square root of the single-particle energy. Also, the excitation energy must be larger than the energy of the first excited state in order for the level density to be defined. Gilbert and Cameron[24] use a composite expression with added shell and pairing correction terms and successfully fit a wide range of data. They found that the Fermi gas model holds well at high excitation energies, which, for heavy thoriumlike nuclei, are found to be above 3–4 MeV.

The Fermi gas model predicts that the level density parameter a is proportional to the mass A. Empirically,[25] this proportionality constant is found to be $\frac{1}{8}$. There are marked deviations from this esti-

mate due to shell effects, particularly near closed shells. Nonetheless, for nuclei near thorium ($A \sim 230-240$), the simple estimate $a = A/8$ compares well with the measured values and is therefore used in the calculations for this work.

A realistic model of the level density is made by using the set of single-particle levels given by the shell model. Rosensweig[26] simulated the shell structure with a bunched periodic system, whereas Moretto *et al.*[27] performed calculations based on the Nilsson model. Nevertheless, at excitation energies above several MeV the shell effects essentially get washed out, and the level density reduces to the Fermi gas model form. The nuclei of interest in this work are not near closed shells, where shell effects are more noticeable, and the range of excitation energies is high ($\sim 3-50$ MeV). Therefore, it is reasonable to use the Fermi gas expression, Eq. (4), for the nuclear level density.

The translational level density is given as $\rho_T(E_f) \sim E_f^{1/2}$ where $E_f = E_i + Q_0 - E^*$ for an incident energy E_i and ground state Q value Q_0. Since the translational density of states varies only with the square root of E^*, while the internal density of states varies with the exponential of the square root of E^*, the translational part of the density is negligible for $E^* \gtrsim 1$ MeV. It remains in the calculations, however, for consistency.

B. One constraint

Surprisal analyis is applied to the energy spectra using the average energy, or centroid of the distribution, as the first constraint. The distribution of maximal entropy $p^{\mathrm{ME}}(E^*)$ is constrained to have the same average energy as the experimental distribution $p(E^*) \sim d^2\sigma/d\Omega\, dE^*$. Therefore,

$$p^{\mathrm{ME}}(E^*) = p^0(E) e^{-\lambda_0 - \lambda E^*} . \tag{5}$$

The rotational and pairing energy corrections turn out to be small (about 1 MeV) compared to the average excitation energy. The average rotational energy E_{rot} imparted to the heavy recoiling nucleus is determined by the average angular momentum transferred by the incident projectile to the heavy nucleus. It is calculated from conservation of angular momentum by orbit matching of classical Coulomb trajectories and assuming zero spin for the light ejectile. The rigid body moment of inertia, I_{rig}, is calculated assuming a spheroidal nucleus of uniform density. An average deformation for thoriumlike nuclei is calculated from measured electric quadrupole moments, so that $I_{\mathrm{rig}} = 1.06 I_{\mathrm{sph}}$, where I_{sph} is the moment of inertia of a sphere with the same mass. As an example, for the grazing reaction ^{232}Th(^{16}O,^{13}C) at an incident energy of 105 MeV, the optimal Q value is -29 MeV, which implies a transferred angular momentum of about $10\hbar$ and a rotational energy of 0.4 MeV. This is small compared to the average excitation energy of 16 MeV.

The calculated value of J for the ^{13}C exit channel is in fair agreement with a value of $11\hbar$ derived from a heavy-ion induced fission measurement[28] of the same system, ^{16}O+^{232}Th at 105 MeV. For the ^{13}C exit channel, as well as for the ^{14}C and ^{15}N exit channels ($J = 8\hbar$ and $7\hbar$), these values of J are close to the values obtained from orbit matching calculations ($J = 9\hbar$ and $5\hbar$).

The pairing energy correction E_{PE} is also relatively small compared to the average excitation energy. For this same example [^{232}Th(^{16}O,^{13}C)^{235}U], $E_{\mathrm{PE}} \simeq 0.78$ MeV. The values of E_{rot} and E_{PE} are given in Table I for all the exit channels of the ^{16}O+^{232}Th reaction at 105 MeV.

A variational procedure[22] is then used to find the distribution of maximal entropy, $p^{\mathrm{ME}}(E^*)$. The one-constraint fits for the exit channels of ^{16}O+^{232}Th at 105 MeV are shown in Fig. 22. The optimal surprisal line is clearly not a least squares fit to the data. This surprisal fit minimizes the Lagrangian L, which is given by[8]

$$L = \sum p(E^*) \ln[p(E^*)/p^{\mathrm{ME}}(E^*)] .$$

Note that in minimizing the deviation between the data and the fit, more importance is given to the more probable data points. For a good fit, $L << \Delta S_{\mathrm{prior}} - S_{\mathrm{exp}}$. $L = 0$, corresponding to a perfect fit, is not attained in practice, either because all the relevant constraints are not included or because of uncertainties in the data. Although the statistical uncertainty of the data is small, the imperfect separation of isotopes may result in systematic errors. In practice, the minimum of L, which is an everywhere-concave function, is determined when its gradient with respect to the parameter(s) is very close to zero. For the one-constraint fits obtained, the minimum value of L ranges from 10^{-1} for the oxygen, nitrogen, and beryllium isotopes, to 10^{-2} for the carbon and boron isotopes. The information content of the experimental distribution, relative to the prior, is about 10–20. The values of $\Delta S(p \mid p^0)$ and $L = \Delta S(p \mid p^{\mathrm{ME}})$ are included in Table I. From Fig. 22, the fits for the boron and carbon exit channels are reasonably good, particularly the fit for ^{12}B with $L = 9 \times 10^{-3}$. In fact, the addition of a second

TABLE I. Measured average excitation energy $\langle E^* \rangle$, squared excitation energy $\langle E^{*2} \rangle$, and square root of excitation energy $\langle E^{*1/2} \rangle$ for the various transfer reaction channels X for the $^{16}O+^{232}Th$ reaction at 105 MeV incident energy and grazing angle 70° laboratory. Also shown are the information contents $\Delta S(p \mid p^0)$ of the experimental distribution and $\Delta S(p \mid p^{ME})$ for distributions of maximal entropy relative to the experimental distributions subject to various constraints, as indicated. The associated Lagrange parameters λ [Eq. (3)] for these distributions are given. The last two columns list the rotational energy E_{rot}, and pairing energy E_{PE} used in Eq. (4).

		One-contraint E^*			Two-constraint E^* and E^{*2}				Two-constraint E^* and $E^{*1/2}$					
X	$\Delta S(p \mid p^0)$	$\langle E^* \rangle$ (MeV)	λ (MeV^{-1})	$\Delta S(p \mid p^{ME})$	$\langle E^{*2} \rangle$ (MeV^2)	λ_1 (MeV^{-1})	λ_2 (MeV^{-2})	$\Delta S(p \mid p^{ME})$	$\langle E^{*1/2} \rangle$ (MeV$^{1/2}$)	λ_1 (MeV^{-1})	λ_2 (MeV$^{-1/2}$)	$\Delta S(p \mid p^{ME})$	E_{rot} (MeV)	E_{PE} (MeV)
^{9}Be	9.2	24.4	1.11	1×10^{-1}	612	0.16	0.019	2×10^{-2}					2.0	0.78
^{10}Be	13	24.2	1.15	1×10^{-1}	600	0.27	0.018	2×10^{-2}					1.8	1.6
^{11}B	18	19.0	1.23	2×10^{-2}	401	1.1	0.0040	7×10^{-3}					1.0	0.78
^{12}B	18	14.8	1.36	9×10^{-3}					3.8	1.4	−0.1	9×10^{-3}	0.86	0.0
^{13}B	15	12.0	1.53	8×10^{-2}					3.4	0.91	4.4	2×10^{-2}	0.77	0.78
^{12}C	22	17.9	1.28	1×10^{-2}					4.2	1.1	1.5	8×10^{-3}	0.51	1.6
^{13}C	22	16.0	1.32	2×10^{-2}					3.9	1.0	2.5	3×10^{-3}	0.38	0.78
^{14}C	24	16.2	1.33	4×10^{-2}					4.0	0.90	3.5	2×10^{-3}	0.33	1.6
^{15}C	19	13.5	1.41	3×10^{-2}					3.6	1.2	1.9	2×10^{-2}	0.17	0.79
^{15}N	31	7.3	1.85	3×10^{-1}					2.5	1.0	5.1	3×10^{-3}	0.078	0.79
^{16}N	24	7.9	1.73	2×10^{-1}					2.7	0.88	4.8	6×10^{-3}	0.006	0.0
^{17}N	20	9.5	1.65	2×10^{-1}					3.0	0.82	5.2	3×10^{-3}	0.001	0.79
^{17}O	26	3.5	2.79	2×10^{-1}					1.8	1.3	6.4	3×10^{-3}	0.032	0.79
^{18}O	20	7.7	1.95	3×10^{-1}					2.7	0.34	9.2	8×10^{-3}	0.089	1.58
^{19}O	13	8.0	1.82	2×10^{-1}					2.7	0.74	6.0	2×10^{-2}	0.22	0.79

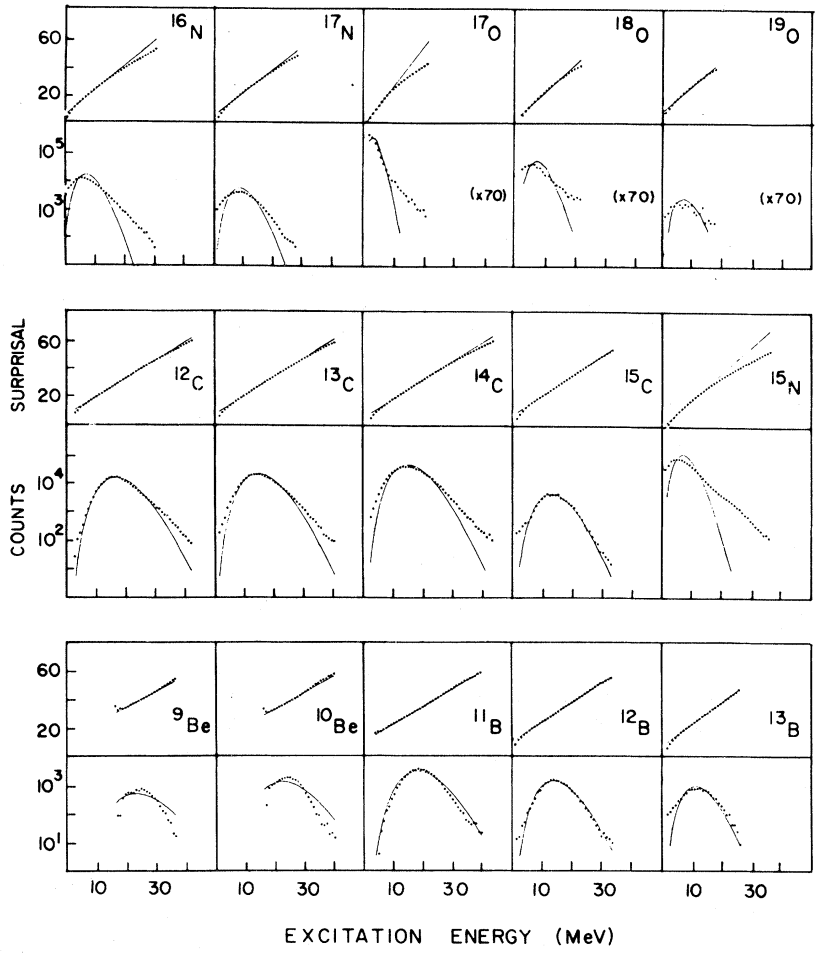

FIG. 22. Energy distributions and surprisal functions for projectilelike products observed at the grazing angle of 70° in the $^{16}O+^{232}Th$ reaction angle at 105 MeV. The curves show the most probable distributions given one constraint on the average excitation energy. The surprisal $I=-\ln[p(E^*)/p^0(E)]$.

constraint does not reduce this value any further. Therefore, as a general guideline, if $L/\Delta S(p\,|\,p^0)\lesssim 10^{-3}$ then the constraint(s) contains essentially all the information of the distribution.

The Lagrange parameters λ are also given in Table I for each of the exit channels. The parameter of the one-constraint fit depends on the most probable energy E^*_{mp} in the following manner[7]

$$\lambda\simeq\sqrt{a/U_{mp}}=\sqrt{a/(E^*_{mp}-E_{rot}-E_{PE})}\,.$$

The parameter λ decreases as the number of transferred nucleons increases, with accordingly higher excitation energy. The value of λ is affected by the energy offset between U_{mp} and E_{mp}, although the qualitative nature of the fit is dominated by the much larger value of the most probable energy.

A large systematic deviation is seen in the surprisal plot of the ^{15}N exit channel in the region of high excitation past $E^*=20$ MeV, indicated by the arrow in Fig. 23. This region has a linear surprisal, with a slope lower than that of the one-constraint fit, which is heavily weighted in the region of low excitation. The reduced slope corresponds to a higher average excitation energy. Figure 23 shows the decomposition of the ^{15}N exit channel into two components, each component corresponding to a linear surprisal. The kink in the spectrum is clearly seen in the logarithmic plot as well as in the surprisal plot. The average excitation energy of the second component is about 15 MeV, which corresponds to an effective optimal Q value of -12 MeV. This is close to the average $Q^{\rm eff}_{\rm opt}$ value of -10 MeV of the other three-nucleon

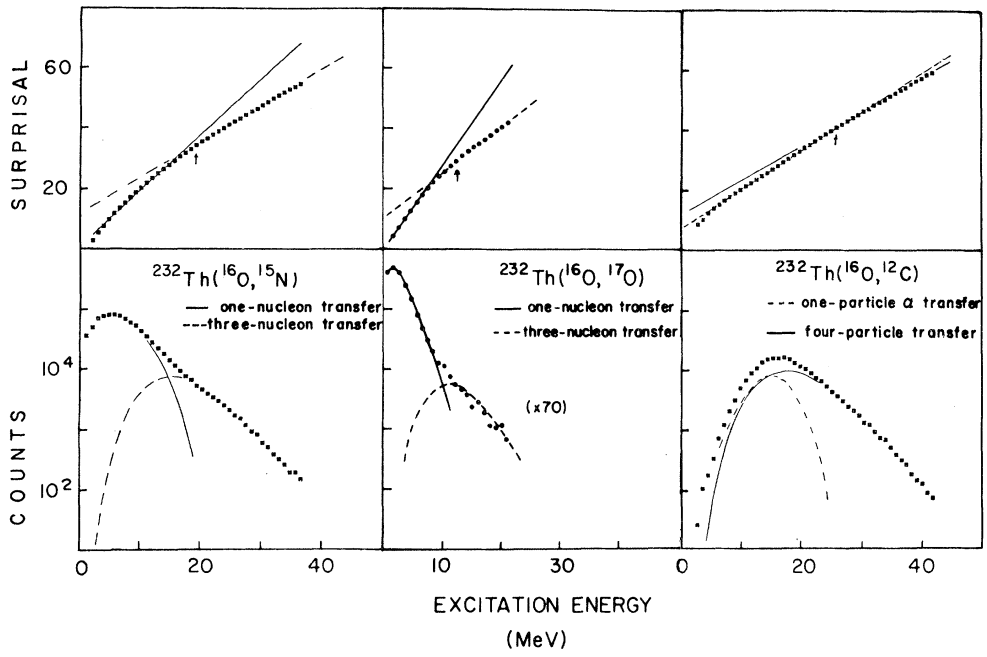

FIG. 23. Energy distributions and surprisal functions for three final channels in the $^{16}O+^{232}Th$ reaction at 105 MeV. The solid and dashed curves show the two components contributing to the transfer in each case, assuming linear surprisals for each component. The three nucleon transfer represents transfer in both directions resulting in only one nucleon net transferred.

transfers. The ratio of the cross section of the second component to that of the first is about 15%. Assuming that the cross section decreases exponentially with ΔN, as in Eq. (2), the relative yield of a three-nucleon transfer, such as ^{13}C, to a one-nucleon transfer should be about 20%, using the observed rate of decrease per nucleon of $e^{-0.8}=0.45$. This suggests that the energy spectrum is composed of two components: a weakly damped one-nucleon transfer, and a more strongly damped three-nucleon transfer, wherein two nucleons are transferred from the projectile to the target and one is transferred in the reverse direction.

One-nucleon pickup to ^{17}O shows the same behavior as one-proton stripping to ^{15}N. The deviation in the surprisal at high excitation energies is clearly seen in Fig. 23, again suggesting a two-component decomposition. The second component, shown as the dotted curve, has an optimal Q value of -13 MeV, close to the expected value for three-nucleon transfer. It represents only 4% of the cross section of the one-nucleon transfer component, in contrast with ^{15}N. The three-nucleon transfer component has a cross section close to those of ^{17}N and ^{15}C. These three nucleon transfer reactions have cross sections that fall off by a factor of 5 in addition to the 20% decrease relative to one-nucleon transfer [see Eq. (2)]; thus, one expects a ratio of only 4%.

The ^{12}C exit channel should also be amenable to this two-component analysis, since the observed deviations of this channel in the variance of the angular distribution, the cross section, and the Q-value dependences upon ΔN suggest a one-particle alpha cluster transfer part of the time. A close look at the surprisal plot does, in fact, reveal a kink at about $E^*=26$ MeV, indicated by the arrow in Fig. 23. Again, each component of the ^{12}C spectrum can be characterized by a linear surprisal, where the more strongly damped four-particle transfer component corresponds to a smaller slope, as indicated by the solid line in Figure 23. This results in a second component with 66% of the cross section and an average excitation energy of 19.5 MeV. These values correspond to a cross section of 2.5 mb/sr and an effective optimal Q value of -12 MeV, which both fall right in line with the systematics for four-particle transfer. The alpha cluster, then, apparently occurs about $\frac{1}{3}$ of the time. The average excitation energy of this component is 14.5 MeV,

which determines the effective optimal Q value to be -7 MeV. The effective optimal Q value of the one-nucleon transfer to ^{15}N and ^{17}O is about -4.5 MeV. It seems likely that other exit channels are also composed of more than one component; however, their surprisals do not easily admit to such a decomposition.

C. Two constraints

The one-constraint fits shown in Fig. 22 accurately account for the decreasing asymmetry of the distribution, going from few-nucleon transfer to many-nucleon transfer; however, the widths of the spectra are not well described. The fits consistently underestimate the widths for few-nucleon transfer and overestimate the widths for many-nucleon transfer. Because the statistical uncertainty in the data is small, the addition of a second constraint is warranted. In theory, one cannot add arbitrary constraints that do not actually exert systematic tendencies on the system, since noninformative constraints do not change the information content of the distribution. In practice, the choice of a physically meaningful contraint must be made carefully since a high quality fit to data with experimental uncertainties is not necessarily unique.

The width of the distribution can be accounted for by constraining the variance, σ^2. Since

$$\sigma^2=\sum p(E^*)(E^*-\langle E^*\rangle)^2 ,$$

a constraint on the variance is equivalent to adding a second constraint on the average value of E^{*2} in addition to the first constraint on the average value of E^*. Then, the distribution of maximal entropy is

$$p^{\mathrm{ME}}(E^*)=p^0(E)\exp(-\lambda_0-\lambda_1E^*-\lambda_2E^{*2}) . \tag{6}$$

The resulting fits are shown in Fig. 24 for ^{9}Be, ^{10}Be, and ^{11}B, the cases of seven-, six-, and five-nucleon transfer, respectively. The minimum values of L for these fits, given in Table I, are about an order of magnitude smaller than those values for the one-constraint fits. Thus, the information content of the experimental distribution relative to the theoretical distribution has been significantly reduced. Both Lagrange parameters, λ_1 and λ_2, are positive, as indicated in Table I. This causes the functional form of Eq. (6) to be close to that of a Gaussian distribution for large E^*. In turn, this accounts for the spectra becoming symmetric for large ΔN, where the average excitation energy is high. This procedure was also applied to the other exit channels where $\Delta N \leq 4$, generating good fits for the other boron isotopes and the carbon isotopes, but not for nitrogen. However, the second parameter in each of these cases is negative, which is suspect since at high energies the term $e^{-\lambda_2E^{*2}}$ eventually

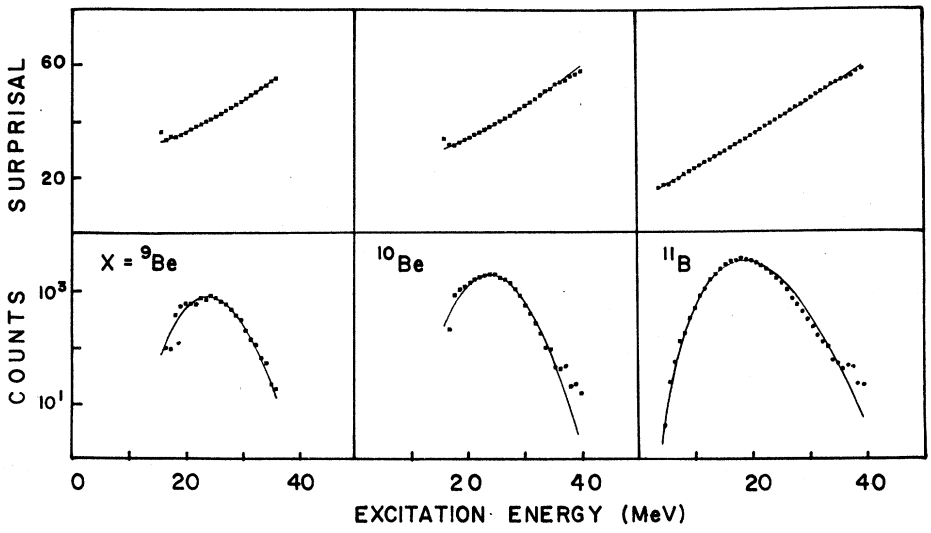

FIG. 24. Energy distributions and surprisal functions for the many nucleon transfer channels in the ^{16}O+^{232}Th reaction at the grazing angle 70° and 105 MeV incident energy. The solid curves show the most probable distributions subject to constraints on the average energy transfer and square energy transfer.

dominates and causes Eq. (6) to be unbound. Therefore, it is questionable that $\langle E^{*2}\rangle$ is the second constraint for small ΔN. Note that for $\Delta N \leq 4$ the one-constraint fit underestimates the width of the observed spectra, whereas for $\Delta N > 4$ the fit overestimates the width. There appears to be a physical constraint limiting the width for large ΔN. One might expect that in addition to the spectra becoming Gaussian shaped as ΔN increases, the distributions would broaden as in a diffusion process. Actually, the variances of the measured spectra do not vary much. In fact, the variance depends only on the charge of the ejectile, increasing from nitrogen to carbon and then decreasing for boron and beryllium. For nitrogen isotopes $\sigma \sim 4.8$ MeV, for carbon $\sigma \sim 5.6$ MeV, for boron $\sigma \sim 4.6$ MeV, and for beryllium $\sigma \sim 3.9$ MeV. σ varies by less than 0.1 MeV among the isotopes of a given charge. It is possible that the Coulomb barrier of the exit channel limits the width of the spectra, all the more so for large mass transfers which are nearly fully damped.

Although some of the data are described very well with the addition of the second constraint on $\langle E^{*2}\rangle$, there could be a different constraint acting on the system, particularly for small ΔN. It has been argued[8] that the width of the exciton distribution, rather than the width of the energy distribution, acts as the second constraint. In terms of the single-particle model, the variance of the exciton distribution about the mean is found to be approximately $(aE^*)^{1/2}$. Therefore, $\langle E^{*1/2}\rangle$ determines the average variance of the exciton distribution.

The distribution of maximal entropy becomes

$$p^{\mathrm{ME}}(E^*) = p^0(E)\exp(-\lambda_0 - \lambda_1 E^* - \lambda_2 E^{*1/2}) , \tag{7}$$

where $\langle E^*\rangle$ is the first constraint and $\langle E^{*1/2}\rangle$ is the second constraint. Figure 25 shows the results of fitting the data with this procedure. All of the exit channels, oxygen through boron, are fit well. The ^{15}N and ^{17}O channels shown are the first one-nucleon transfer components. The values of λ_2, included in Table I, range from about 9 for ^{18}O to about 0 for ^{12}B. A troublesome point is that, for the form of Eq. (7) to account for the symmetric beryllium channels, the Lagrange parameter λ_2 must go to very large negative values (so large that the program has trouble finding the solution). However, a search for large negative values of λ_2 seems more symptomatic of a problem with the constraint than with the computer program. In this case, the dominant term $e^{-\lambda_1 E^*}$ keeps Eq. (7) from being unbound at high E^*, although it seems unlikely that large negative values of λ_2 could be meaningful. For this reason, the cases of ^{9}Be, ^{10}Be, and ^{11}B, discussed previously, will not be considered further.

Because the prior distribution depends exponentially on the square root of E^*, the form in Eq. (7) can be rewritten in the form of a one-constraint distribution.[8] Defining $a^* = (a^{1/2} - \lambda_2/2)^2$, then

$$\lambda_1 \simeq (a^*/E^*_{\mathrm{mp}})^{1/2} ,$$

$$\lambda_2 \simeq 2a^{1/2} - (22E^{*3/2}_{\mathrm{mp}}/\Delta E^{*2}) ,$$

where E^*_{mp} is the most probable excitation energy (approximately the mean excitation energy), and ΔE^* is the full width at half maximum of the energy distribution. Rewriting the approximation for the second parameter λ_2,

$$(a^* E^*_{\mathrm{mp}})^{1/2} \simeq 11(E^*_{\mathrm{mp}}/\Delta E^*)^2 . \tag{8}$$

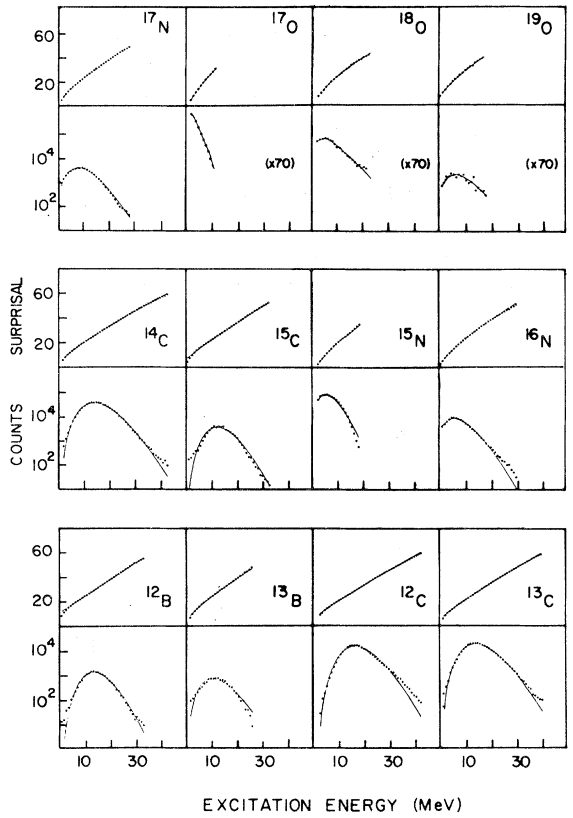

FIG. 25. Energy distributions and surprisal functions for the projectilelike products observed at the grazing angle 70° in the ^{16}O+^{232}Th reaction at 105 MeV incident energy. The solid curves show the most probable distributions subject to constraints on the average energy transfer and on the average square root of the excitation energy.

Therefore, the second constraint is related to the relative values of the average excitation energy and the width of the distribution.

The experimental values of $(E^*_{mp}/\Delta E^*)^2$ are plotted in Fig. 26 as a function of ΔN in the upper left corner for the $^{16}O+^{232}Th$ reaction. The solid curves are drawn to guide the eye. These values are seen to be nearly independent of the specific nature of the ejectile, increasing smoothly with ΔN, as indicated by the solid curve that guides the eye. The rate of increase is greater than $(E^*_{mp})^{1/2}$; therefore, a^* also increases with ΔN, which causes λ_2 to decrease. This is the observed behavior. The parameter a^* can be regarded as an effective level density parameter, which is seen to decrease for few-nucleon transfer. This view, however, is not valid if λ_2 were allowed to be negative, since then a^* would become larger than a. As mentioned, these cases are not considered.

The two-constraint analysis was applied to the other measured reactions to see if the systematic changes would be consistent with the discussion thus far. With constraints on $\langle E^* \rangle$ and $\langle E^{*1/2} \rangle$, the energy spectra for the $^{16}O+^{232}Th$ grazing reactions at different bombarding energies are well described.

The second parameter λ_2 increases monotonically for each exit channel as the incident energy increases. Also, λ_2 goes from negative to positive for

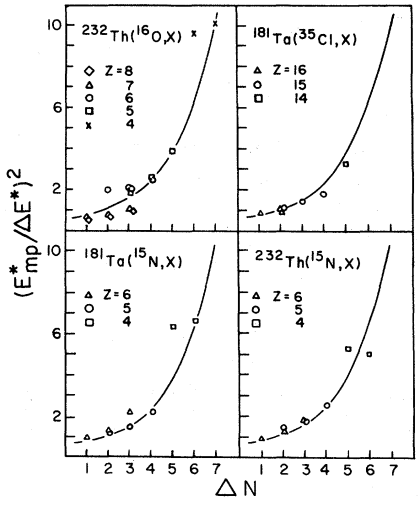

FIG. 26. The square of the most probable energy divided by the width of the energy distribution as a function of the number of transferred nucleons ΔN for four selected reactions. The curve is to guide the eye, but is the same in each of the four panels.

^{11}B, ^{12}C, and ^{13}C, as the energy increases from 97 to 125 MeV. This is basically a consequence of the changing ratio of the centroid of the energy distribution to its width. In terms of Eq. (8), this ratio determines $(a^*E^*_{mp})^{1/2}$, where a^* decreases as λ_2 increases. The experimental values of $(E^*_{mp}/\Delta E^*)^2$ are approximately constant with bombarding energy for each exit channel, perhaps decreasing slightly with increasing energy. Since E^*_{mp} increases with bombarding energy, a^* decreases, which accounts for larger values of λ_2. Thus, the behavior of the effective level density parameter suggests that the available phase space is more restricted as the interaction time decreases with higher bombarding energies. For example, in the one-nucleon transfer to ^{15}N, a^* decreases from 7.3 MeV^{-1} at $E_{lab}=97$ MeV to a value of 2.4 MeV^{-1} at $E_{lab}=125$ MeV. The parametrized Fermi gas level density parameter a, for this case, is 29.1 MeV^{-1}.

The spectral shapes also vary with scattering angle. The ratio $(E^*_{mp}/\Delta E^*)$ increases with θ_{lab} for each exit channel, which causes a^* to increase and, therefore, λ_2 to decrease. At $E_{lab}=105$ MeV, λ_2 goes from positive to negative for ^{12}C, ^{13}C, and ^{14}C, as θ_{lab} increases from 60° to 100°. Again, considering the one-nucleon transfer to ^{15}N, a^* increases from 3.3 MeV^{-1} at $\theta_{lab}=60°$ to 12 MeV^{-1} at $\theta_{lab}=100°$. This suggests that the available phase space is less restricted for more strongly damped collisions, which scatter to backward angles. Thus, at 100° the spectra for all of the exit channels, except ^{15}N, are nearly Gaussian distributions. Since these ejectiles are almost fully damped, as indicated in Fig. 9, the widths may be constrained. A fit with constraints on $\langle E^* \rangle$ and $\langle E^{*2} \rangle$ works well for these cases.

A sampling of the results for the other systems is indicated in Table II as a comparison with the $^{16}O+^{232}Th$ reaction. Similarly, the parameter λ_2 decreases as ΔN increases for these grazing reactions: $^{15}N+^{181}Ta$ at 86 MeV, $^{15}N+^{232}Th$ at 95 MeV, and $^{35}Cl+^{181}Ta$ at 205 MeV. The ratios $(E^*_{mp}/\Delta E^*)^2$ as a function of ΔN, are nearly independent of the choice of colliding ions, increasing with ΔN at a similar rate for all three reactions. The curves drawn in the four panels of Fig. 26 are identical. The average excitation energy of a one-nucleon transfer for $^{35}Cl+^{181}Ta$ is about 16 MeV, which is twice that of a one-nucleon transfer for $^{16}O+^{232}Th$; still, the widths of the energy distributions scale accordingly. Therefore the shapes of the distributions, as well as the average energies about which the distributions are peaked, depend mainly

TABLE II. Lagrange parameters for distributions of maximal entropy subject to two constraints on $\langle E^* \rangle$ and $\langle E^{*1/2} \rangle$, Eq. (7), for various grazing reactions, as indicated.

X	$^{15}N+^{181}Ta$ 86 MeV λ_1 (MeV^{-1})	λ_2 ($MeV^{-1/2}$)	$^{15}N+^{232}Th$ 95 MeV λ_1	λ_2	X	$^{35}Cl+^{181}Ta$ 205 MeV λ_1	λ_2
^{11}B	1.1	0.96	1.1	1.9	^{30}Si	0.51	3.4
^{12}B	1.4	0.70	1.1	3.5	^{32}P	0.43	4.9
^{13}B	0.95	4.6	0.94	5.5	^{33}P	0.39	5.5
^{12}C	0.92	2.0	0.86	3.8	^{33}S	0.32	6.3
^{13}C	0.91	3.0	0.97	3.5	^{34}S	0.42	6.1
^{14}C	0.83	4.7	0.77	5.6	^{35}S	0.40	5.5
^{15}C			0.99	4.1	^{36}Cl	0.85	3.8
					^{37}Cl	0.57	4.8

on the number of transferred nucleons, rather than the particular interacting nuclei. Surprisal analysis, then, can serve as a general description of continuum energy spectra for transfer reactions, at least within the limits discussed here.

Further consideration must be given to the origin of the second constraint, be it $\langle E^{*1/2} \rangle$ or $\langle E^{*2} \rangle$. A calculation was done[9] to test the possibility that a constraint on the average transferred angular momentum manifests itself as an energy-dependent constraint. A constraint on angular momentum implies that the average value of J is constrained to be smaller than the yrast value, which limits the available phase space, especially for few-nucleon transfer where the average transferred angular momentum is small. If $\langle J \rangle$ acts as the second constraint, however, its influence on the data is averaged, since the measured cross section averages over the angular momentum-dependent cross section. The calculation, in fact, produces only a different normalization, or a very weak energy dependence for large angular momentum transfers.

V. SUMMARY AND CONCLUSIONS

The results of the preceding sections are summarized here. The $^{16}O+^{232}Th$ transfer reaction is studied in detail and compared with other systems, including $^{15}N+^{232}Th$, $^{15}N+^{181}Ta$, and $^{35}Cl+^{181}Ta$. The reactions studied are highly asymmetric, in order to unambiguously determine the final reaction products. A systematic investigation is made of the reactions as a function of bombarding energy and scattering angle, so as to vary the incident velocity at the distance of closest approach (where transfer presumably takes place) and the depth of penetration during transfer. The general features of these reactions, including energy dissipation and the branching ratio of the exit channels, are found to be very similar for the different systems. These properties depend mainly on the number of transferred nucleons, ΔN, rather than the specific nature of the colliding ions.

The measured energy distributions for each exit channel can be characterized by the average energy about which the distribution is peaked, the width, and the degree of asymmetry. The energy spectra are asymmetric for few-nucleon transfer, becoming symmetric as ΔN increases. For large ΔN, the distributions are nearly Gaussian shaped, although the widths do not broaden as a diffusion model would predict. The effective optimal Q value is observed to decrease smoothly with ΔN to the fully damped, or completely relaxed, limit. A semiclassical damping model accounts for the optimal Q values of the grazing reactions. It allows a phenomenological velocity-dependent frictional force to act during the transfer of nucleons. The interaction time is assumed to scale as $\Delta N/v$, where v is the average velocity at the distance of closest approach. The damping coefficient, which determines the rate of damping, is found to be constant for all exit channels, up to $\Delta N = 7$. In fact, the constant is independent of entrance channel as well, even as the projectile doubles in size from ^{16}O to ^{35}Cl. Therefore, the grazing reactions of these systems can all be charac-

terized by the same relative rate of energy damping. At the highest energies, however, the model overestimates the measured energy loss as ΔN increases; thus, the damping coefficient, or the interaction time for each nucleon transfer, appears to decrease for large ΔN. The average energy loss for collisions that scatter backward of the grazing angle can also be accounted for. Here, the more strongly damped collisions require a larger damping coefficient, which may be due to a larger region of overlap of the nuclear surfaces than that for a grazing reaction.

The energy spectra are integrated to yield the branching ratios of the exit channels. Here, too, a systematic dependence with ΔN is observed. The cross section is found to decrease exponentially with ΔN. The sequence of nucleon transfer is considered to be a statistical process, with each additional nucleon transfer having the same probability of occurrence. The probability for the production of certain isotopes is diminished relative to those along the energetically dominant sequence, which can be related to a difference in the reaction energetics. The cross section of the $(2p,2n)$ transfer is anomalously high, which may be due to the clustering of an alpha particle about one-third of the time, making transfer more probable. For grazing reactions at higher energies, the linear relation of $\ln(d\sigma/d\Omega)$ as a function of ΔN still holds, although the magnitude of the average slope decreases, causing many-nucleon transfer to be more favorable relative to few-nucleon transfer. Similarly, for collisions that scatter forward or backward of the grazing angle, the systematic dependence tends to level out and, in general, is not as smooth a dependence as for the grazing reaction.

The energy spectra are examined in terms of a constrained phase-space approach. The measured energy distribution is considered to be of maximal entropy, subject to one or two constraints. The available phase space is assumed to be that of a Fermi gas distribution. It is empirically found that a single constraint on the average of the distribution results in a good description of some distributions. The widths and asymmetries of the spectra are accounted for with the one-constraint fits. Therefore, the average energy contains most of the information content of the distribution. The constraint is interpreted to be a consequence of the influence of the optimal Q value upon the reaction. Systematic deviations, however, are seen in the fits, for both small and large ΔN. For one-nucleon transfer, including ^{232}Th(^{16}O,^{15}N) and ^{232}Th(^{16}O,^{17}O), a two-component analysis of the spectra implies the coexistence of a weakly damped one-nucleon transfer and a more strongly damped three-nucleon bidirectional transfer. The ^{12}C exit channel, as well, was separated into two components: a four-particle $(2p,2n)$ transfer and an alpha particle cluster transfer, which occurs 34% of the time. The anomalies of the ^{12}C channel in the variance of the angular distributions, the cross-section systematics, and optimal Q-value systematics are then accounted for.

Since the statistical uncertainties in the data are small, an attempt is made to introduce a second constraint. The asymmetric distributions for few-nucleon transfer can be described with a second constraint on the average square root of the excitation energy. The two-constraint fits reduce the information content of the experimental distribution relative to the theoretical distribution by an order of magnitude. This is not, however, amenable to a simple interpretation. One suggestion is that the constraint on $\langle E^{*1/2}\rangle$ is related to a constraint on the variance of the exciton distribution. Another is that it results from a constraint on the average angular momentum, though this could not be demonstrated. It is, however, consequential that a wide range of data can be described in terms of this approach with constraints on $\langle E^{*}\rangle$ and $\langle E^{*1/2}\rangle$, particularly for high quality data. On the other hand, this procedure does not appear meaningful for many-nucleon transfer, where the symmetric energy spectra are best described in terms of a second constraint on $\langle E^{*2}\rangle$ related to the variance of the energy distribution. Although one might question the validity of using a Fermi gas distribution to describe the available phase space, the region of excitation energies considered here is relatively high and the same form of the level density distribution accounts for a wide range of reactions investigated.

In conclusion, the transfer reactions considered here are amenable to a statistical approach— specifically the energy distributions and the energy-integrated yields. The yields have a simple dependence on ΔN that is more pronounced than the Q_0 systematics observed by Artukh *et al.*[4] Surprisal analysis has proved useful in several ways. It provides a description of the data that allows one to compare different reactions easily and to spot systematic differences, such as those that led to a two-component analysis for several exit channels. The analysis with constraints on $\langle E^{*}\rangle$ and $\langle E^{*1/2}\rangle$, which describes most of the data very well, implies that these two constraints contain essentially all the

information content of the energy distribution. Therefore, a relatively simply dynamical interpretation of the data should be possible.

ACKNOWLEDGMENTS

The authors wish to thank the following for their help with the data collection: Dr. J. Ball, Dr. T. Belote, Dr. A. Lazzarini, Dr. D. Perlman, G. Garfunkel, and D. Ila. Discussions with Dr. R. Levine, Dr. Y. Alhassid, and Dr. A. Winther are also greatly appreciated. F.V. thanks the Danish Natural Science Research Council for support. S.G.S. thanks the General Electric Company for a young faculty career development grant. This research was sponsored by the U. S. Department of Energy under Contract No. DE-AC02-76-ER03069.

---

*Present address: Physics Department, SUNY at Stony Brook, Stony Brook, New York 11794.

[1]T. Udagawa, B. T. Kim, and T. Tamura, Proceedings of the IPCR Symposium on Macroscopic Features of Heavy-Ion Collisions and Pre-Equilibrium Process, Hakone, 1977, edited by H. Kamitsubo and M. Ishihara, IPCR Cyclotron Progress Report, Wako-shi, Saitama, 1977, p. 3.

[2]W. Nörenberg, Phys. Lett. 52B, 289 (1974).

[3]V. V. Volkov, *Proceedings of the International Conference on Reactions Between Nuclei, Nashville, 1974,* edited by R. L. Robinson, F. K. McGowan, J. B. Ball, and J. H. Hamilton (North-Holland, Amsterdam, 1974), Vol. II, p. 363.

[4]A. G. Artukh, V. V. Avdeichikov, J. Ero, G. F. Gridnev, V. L. Mickheev, V. V. Volkov, and J. Wilczynski, Nucl. Phys. A160, 511 (1971).

[5]J. P. Bondorf, F. Dickmann, D. H. E. Gross, and P. J. Siemans, J. Phys. C 6, 145 (1971).

[6]S. Y. Lee and P. Braun-Munzinger, Phys. Rev. C 24, 1343 (1981).

[7]R. D. Levine, S. G. Steadman, J. S. Karp, and Y. Alhassid, Phys. Rev. Lett. 41, 1537 (1978).

[8]Y. Alhassid, R. D. Levine, J. S. Karp, and S. G. Steadman, Phys. Rev. C 20, 1789 (1979).

[9]J. S. Karp, Ph.D. thesis, Massachussets Institute of Technology, 1980 (unpublished).

[10]A. H. Wapstra and N. B. Gove, Nucl. Data Tables A9, 265 (1971).

[11]K. Rubin, B.S. thesis, Massachusetts Institute of Technology, 1978 (unpublished).

[12]F. C Perey (unpublished); modified to heavy ion, F. Videbaek (unpublished).

[13]W. G. Meyer, R. G. Clark, V. E. Viola, Jr., R. G. Sextro, and A. M. Zebelman, Z. Phys. A 277, 141 (1976).

[14]W. U. Schröder and J. R. Huizenga, Annu. Rev. Nucl. Sci. 27, 465 (1977).

[15]J. S. Blair, Phys. Rev. 95, 1218 (1954).

[16]P. J. A. Buttle and L. J. B. Goldfarb, Nucl. Phys. A176, 299 (1971).

[17]T. Mikumo, I. Hohno, K. Katori, T. Motobayashi, S. Nakajima, S. Yoshie, and H. Kamitsubo, Phys. Rev. C 14, 1458 (1976).

[18]F. C. Tsang, Phys. Scr. 10A, 90 (1974).

[19]F. Videbaek, R. B. Goldstein, L. Grodzins, S. G. Steadman, T. A. Belote, and J. D. Garrett, Phys. Rev. C 15, 954 (1977).

[20]R. D. Levine and R. B. Bernstein, *Dynamics of Molecular Collisions,* edited by W. H. Miller (Plenum, New York, 1975), Part B, p. 323–364.

[21]E. T. Jaynes, Phys. Rev. 106, 620 (1957).

[22]Y. Alhassid, N. Agmon, and R. D. Levine, Chem. Phys. Lett. 53, 22 (1978).

[23]A. Bohr and B. R. Mottleson, *Nuclear Structure* (Benjamin, New York, 1969).

[24]A. Gilbert and A. G. W. Cameron, Can. J. Phys. 43, 1446 (1965).

[25]J. R. Huizenga and L. G. Moretto, Annu. Rev. Nucl. Sci. 22, 427 (1972).

[26]N. Rosensweig, Phys. Rev. 105, 950 (1957).

[27]L. G. Moretto, R. Stella, and V. Caramella-Crespi, Energ. Nucl. 17, 436 (1970).

[28]J. S. Karp, G. G. Batrouni, L. Grodzins, S. G. Steadman, and F. Videbaek, Proceedings of the International Symposium on Physics and Chemistry of Fission, Julich, 1979.